

Circuits with broken fibration symmetries perform core logic computations in biological networks

Ian Leifer¹, Flaviano Morone¹, Saulo D. S. Reis², José S. Andrade, Jr.²,
Mariano Sigman³, Hernán A. Makse^{1*}

1 Levich Institute and Physics Department, City College of New York, New York, New York, USA

2 Departamento de Física, Universidade Federal do Ceará, Fortaleza, Ceará, Brazil

3 Laboratorio de Neurociencia, Universidad Torcuato Di Tella, Buenos Aires, Argentina

* hmakse@ccny.cuny.edu

Abstract

We show that logic computational circuits in gene regulatory networks arise from a fibration symmetry breaking in the network structure. From this idea we implement a constructive procedure that reveals a hierarchy of genetic circuits, ubiquitous across species, that are surprising analogues to the emblematic circuits of solid-state electronics: starting from the transistor and progressing to ring oscillators, current-mirror circuits to toggle switches and flip-flops. These canonical variants serve fundamental operations of synchronization and clocks (in their symmetric states) and memory storage (in their broken symmetry states). These conclusions introduce a theoretically principled strategy to search for computational building blocks in biological networks, and present a systematic route to design synthetic biological circuits.

Author summary

We show that the core functional logic of genetic circuits arises from a fundamental symmetry breaking of the interactions of the biological network. The idea can be put into a hierarchy of symmetric genetic circuits that reveals their logical functions. We do so through a constructive procedure that naturally reveals a series of building blocks, widely present across species. This hierarchy maps to a progression of fundamental units of electronics, starting with the transistor, progressing to ring oscillators and current-mirror circuits and then to synchronized clocks, switches and finally to memory devices such as latches and flip-flops.

Introduction

In all biological networks [1] some simple ‘network motifs’ appear more often than they would by pure chance [2–4]. This regularity has been interpreted as evidence that these motifs are basic building blocks of biological machineries, a proposal that has had a major impact on systems biology [4, 5]. However, mere statistical abundance by itself does not imply that these circuits are core bricks of biological systems. In fact, whether these network motifs may have a functional role in biological computation remains controversial [6–9].

Functional building blocks should offer computational repertoires drawing parallels between biological networks and electronic circuits [10]. Indeed, the idea of using electronic circuitry and devices to mimic aspects of gene regulatory networks has been in circulation almost since the inception of regulatory genetics itself [11]. This idea has been a driving force in synthetic biology [12]; with several demonstrations showing that engineered biological circuits can perform computations [13], such as toggle switches [14–17], logic [18], memory storage [15, 19, 20], pulse generators and oscillators [14, 21–23].

In a previous work [24], we have shown that the building blocks of gene regulatory networks can be identified by the fibration symmetries of these networks. In the present paper, we first demonstrate the functionality of these symmetric building blocks in terms of synchronized biological clocks. We then show that the breaking of the fibration symmetries of the network identifies additional building blocks with core logic computational functions. We do so through a constructive procedure based on symmetry breaking that naturally reveals a hierarchy of genetic building blocks widely present across biological networks and species. This hierarchy maps to a progression of fundamental units of electronics, starting with the transistor, and progressing to ring oscillators and current-mirror circuits and then to memory devices such as toggle switches and flip-flops. We show that, while symmetric circuits work as synchronized oscillators, the breaking of these symmetries plays a fundamental role by switching the functionality of circuits from synchronized clocks to memory units.

Thus, our constructive theoretical framework identifies 1) building blocks of genetic networks in a unified way from fundamental symmetry and broken symmetry principles, which 2) assure that they perform core logic computations, 3) suggests a natural mapping onto the foundational circuits of solid state electronics [12, 13], and 4) endows the mathematical notion of symmetry fibration [24] with biological significance.

Results

Feed-forward loops do not synchronize

We start our analysis by considering the dynamics of the most abundant network motif in transcriptional regulatory networks, the so-called feed-forward loop (FFL) introduced by Alon and coworkers [3, 4, 25]. A cFFL motif consists of three genes (X, Y and Z; c refers to coherent where all regulators are activators) where the transcription factor expressed by gene X positively regulates the transcription of Y and Z, and, in turn Y regulates Z (Fig. 1A). Fig. 1A shows an example of cFFL motif in *E. coli* with $X=cpxR$, $Y=baeR$, and $Z=spy$. Numerical and analytic solutions for the expression levels of the genes in the cFFL (Fig. 1B) demonstrate that the FFL does not reach synchronization (unless for very specific setting of parameters) nor oscillations in expression levels. This is consistent with previous research which has interpreted the functionality of the FFL as signal delay [3, 25, 26].

We illustrate this result by presenting an analytical solution of the FFL [2–4]. We use a discrete time, continuous state variable model with a logic Boolean interaction function in the spirit of the Glass and Kauffman model of biochemical networks [27]. The dynamics of the expression levels y_t and z_t of genes Y and Z, respectively, as a function of time t in the cFFL is given by the following difference equations [4]:

$$\begin{aligned} y_{t+1} &= (1 - \alpha)y_t + \gamma_x \theta(x_t - k_x), \\ z_{t+1} &= (1 - \alpha)z_t + \gamma_x \theta(x_t - k_x) \times \gamma_y \theta(y_t - k_y), \end{aligned} \quad (1)$$

where x_t is the expression level of gene X, α is the degradation rate of the gene, γ_x and γ_y are the strength of the interaction representing the maximum expression rate of

genes X and Y, respectively, and the thresholds k_x and k_y are the dissociation constant between the transcription factor and binding site. The expression level is measured in terms of abundance of gene product, e.g., mRNA concentration. The Heaviside step functions $\theta(x_t - k_x)$ and $\theta(y_t - k_y)$ represent the activator regulation from gene X and Y, respectively. They represent the Boolean logic approximation of Hill input functions in the limit of strong cooperativity [4, 27]. We consider an AND gate for the combined interaction of transcription factors of genes X and Y onto the binding sites of gene Z [4]. Analogous results shown in S1 File Section I can be obtained with an OR gate and with ODE continuum models.

In S1 File Sec. I A, we show that the expression levels of the genes Y and Z do not synchronize, in other words, $y_t \neq z_t, \forall t$. For example, Fig. 1B shows a particular set of parameters which results in a non-synchronized state. Such state is obtained under initial condition $y_0 > k_y$ and $\alpha < \gamma_x$. Specifically, we use the parameters: $\alpha = 0.2$, $\gamma_x = 0.12$, $\gamma_y = 0.7$, $k_x = 0.5$ and $k_y = 0.1$. For this combination, y_t and z_t do not synchronize since y_t saturates at $y_t \rightarrow \gamma_x/\alpha = 0.6$ when $t \rightarrow \infty$, and z_t saturates at $z_t \rightarrow \gamma_x\gamma_y/\alpha = 0.42$, for $t \rightarrow \infty$. In this figure, we set x_t equal to a square wave and then monitor the expression levels of y_t and z_t . When $x < k_x$, both y_t and z_t decay exponentially to zero. On the other hand, when $x > k_x$, both variables evolve to saturate again at $y_t = \gamma_x/\alpha$ and $z_t = \gamma_x\gamma_y/\alpha$, in agreement with the analytical solution.

Feed-forward fibers synchronize via a symmetry fibration

In the FFL, gene Z receives input from X and Y, while gene Y, instead, only from X, and therefore the inputs are not symmetric (Fig. 1C). But as it turns out, a search of motifs in biological networks [24] shows that the FFL circuit in Fig. 1A regularly appears in conjunction with an autoregulation (AR) loop [28] at $Y=baeR$ (Fig. 1E). This minimal inclusion in the FFL symmetrizes the circuit and we show, next, that this symmetry results in a circuit with a first and minimal form of function: synchronization in gene expression. This can be formalized by analyzing invariances in the input tree [24], which represents all the paths that converge to a given gene (Fig. 1C and G). The mathematical principle of symmetry fibration in dynamical systems introduced in [24, 29, 30] predicts this, since symmetries $Y \leftrightarrow Z$ that leave invariant the tree of inputs (but not necessarily the outputs as imposed by automorphisms) are necessary and sufficient to achieve synchronization. When two genes have isomorphic input trees, their expression levels are synchronized, see [24] for details.

For instance, by means of its autoregulation, *baeR* forms a symmetry fibration with gene *spy*, that can be formalized and characterized by an isomorphism between the input trees of these genes (Fig. 1G). When two input trees, like those of *baeR* and *spy*, are isomorphic, the expression levels of these two genes are synchronized. These genes are said to belong to the same ‘*fiber*’ [24, 30]. Genes in the same *fiber* are redundant, and can be collapsed into the ‘*base*’ (see Fig. 1H) by a symmetry fibration [24] (the FFL, instead, cannot be reduced since it has no symmetry, see Fig. 1D). Numerical simulations and analytical solutions (Fig. 1F, S1 File Section II A and Section II B) confirm that the addition of the AR loop to the FFL – leading to a circuit that we call the Feed-Forward Fiber (FFF) – changes its functionality qualitatively, leading to synchronization of genes Y and Z into coherent co-expression. This prediction is confirmed with experimental co-expression profiles in Ref. [24].

The FFF with activator regulations in Fig. 1E has a simple dynamics converging to a synchronized fixed point: all interactions are satisfied meaning that the Heaviside step functions evaluate to 1 and we call this circuit SAT-FFF. Instead, when the autoregulation is a repressor, the loop behaves as a logical NOT gate. When expression is high it inhibits itself shifting to low state. Instead, if it is low it promotes itself to shift to a high state. Hence, the activity of this gene oscillates indefinitely [14, 27]. This is

the simplest expression of *frustration* [27,31], a core concept in physics which refers to a system which is always in tension and thus never reaches a stable fixed configuration.

A biological transistor as a core building block

To understand the computation rationale of symmetric and frustrated circuits made of repressors, we map them to electronic analogues. We begin the analogy with the simplest circuit of a single gene with a feedback loop with repression (AR loop, Fig. 2D). The dynamics for the expression level y_t is described by the discrete time model with Boolean interaction [27]:

$$\Delta y_t = y_{t+1} - y_t = -\alpha y_t + \gamma_y \theta(k_y - y_t). \quad (2)$$

Here, α is the degradation rate of the Y gene product, γ_y is the maximum expression rate of gene Y, and k_y is the dissociation constant.

The Heaviside step function $\theta(k_y - y_t)$ reflects the repressor autoregulation in the Boolean logic approximation. We will show that this genetic repressor interaction, shown as the stub in Fig. 2B, is the genetic analogue of a solid-state transistor shown in Fig. 2A.

A transistor is typically made up of three semiconductors, a base sandwiched between an emitter and a collector (Fig. 2A). The current flows between the emitter and collector only if voltage applied to the base is lower than at the emitter ($V_B < V_E$) and thus the transistor acts as a switch and inverter. In the genetic circuit, the expression y_t drives the rate of expression of gene Y, like the voltage drives current around an electric circuit. Simply comparing Eq. (2) to the pnp transistor in Fig. 2A leads to the analogy in which the expression y_t is an analogue for the base potential V_B of a transistor, k_y an analogue for V_E , γ_y an analogue for the emitter current I_E , αy_t an analogue for I_B , and Δy_t an analogue for I_C . Then, Eq. (2) provides the genetic equivalent of the equation for a transistor's collector current $I_C = I_E - I_B$ (Fig. 2C, D).

The repressor AR genetic circuit of Fig. 2D becomes a one-stage ring oscillator (Fig. 2C) where the collector of the transistor connects to the base forming the minimal signal feedback loop. As shown in Fig. 2D, an example of the AR is the gene Y = *trpR* from the *E. coli* transcriptional network. The repressor AR loop can be extended to the FFF by symmetrizing it, adding gene Z, such that it synchronizes with Y to express an enzyme that catalyzes a biochemical reaction (Fig. 2F). The circuit is completed with the external regulator X which keeps the symmetry between Y and Z. The resulting circuit is called UNSAT-FFF (since it is frustrated).

The UNSAT-FFF maps to the so-called Widlar current-mirror electronic circuit shown in Fig. 2E, a popular building block of integrated circuits used since the foundations of the semiconductor industry (1967 US patent [32,33]). It serves two key functions as we show below: mirror synchronization of $y_t = z_t$ and oscillatory activity (Fig. 2G and S1 File Section III).

UNSAT-FFF solution oscillates and synchronizes

Next, we show analytically and numerically that the UNSAT-FFF circuit has an oscillatory solution plus synchronization of genes Y and Z. S1 File Section III A shows that the prediction of oscillatory behavior can be obtained also from a model of gene expression in the continuum time-domain using a first-order ODE model with time delay due to the process of transcription and translation. Below, we focus on the discrete dynamics.

The UNSAT-FFF circuit is obtained by the addition of a repressor AR loop to the FFL: in Fig. 2F, gene Y acts as a repressor regulator on the gene Z and on itself. There

are many variants of this circuit depending on the combinations of activator and repressor regulators. Here, we use X gene as an activator and Y gene as a repressor. Different variants yields analogous results and will be discussed elsewhere. The important ingredient is the existence of frustration in the interactions. For instance if gene X is high, then it will make genes Y and Z high too. However, this configuration does not satisfy the repressor autoregulation bond neither the repression from Y \rightarrow Z. Thus, two bonds are unsatisfied and this circuit unsatisfied: UNSAT-FFF. The discrete-time dynamics of the expression levels of genes y_t and z_t are given by:

$$\begin{aligned} y_{t+1} &= (1 - \alpha)y_t + \gamma_x\theta(x_t - k_x) \times \gamma_y\theta(k_y - y_t) , \\ z_{t+1} &= (1 - \alpha)z_t + \gamma_x\theta(x_t - k_x) \times \gamma_y\theta(k_y - y_t) , \end{aligned} \quad (3)$$

where γ_x and γ_y are the strength of the interaction (maximum expression rate) of genes X and Y, respectively, and k_x and k_y are the dissociation constant, respectively. Similarly to the SAT-FFF case, synchronization between y and z occurs for the UNSAT-FFF (see S1 File Section II). However, the impact of the repressor feedback loop on the dynamical behavior of this circuit is more profound, since it leads to oscillations. Thus, while both, SAT-FFF and UNSAT-FFF, lead to synchronization of Y and Z, the former synchronizes into a fixed point and the later into an oscillatory limit cycle.

We set $\lambda = \gamma_x\gamma_y/k_y\alpha$, and $\beta = 1 - \alpha$, so that we rewrite Eq. (3) for the rescaled variables $\psi_t = y_t/k_y$ and $\zeta_t = z_t/k_y$ as

$$\begin{aligned} \psi_{t+1} &= \beta\psi_t + \alpha\lambda\theta(x_t - k_x)\theta(k_y - \psi_t), \\ \zeta_{t+1} &= \beta\zeta_t + \alpha\lambda\theta(x_t - k_x)\theta(k_y - \psi_t). \end{aligned} \quad (4)$$

Now, we set $x_t = x$ constant in time for simplicity. For $x < k_x$, the solutions exponentially decay as $\psi_t = \psi_0 e^{-t/\tau}$ and $\zeta_t = \zeta_0 e^{-t/\tau}$, where ψ_0 is the initial condition. For $x > k_x$, Eq. (4) defines an iterative map which satisfies the following recursive equation:

$$f^t(\psi) = f^{t-1}(\beta\psi)\theta(\psi - 1) + f^{t-1}(\beta\psi + \alpha\lambda)\theta(1 - \psi). \quad (5)$$

This iterative map results in different solutions depending on the value of λ .

We consider first the case where the initial condition is $\psi_0 > 1$. Thus, the solution of Eq. (4) is $\psi_t = \psi_0 e^{-t/\tau}$, where $\tau^{-1} = -\log(1 - \alpha)$. This solution is correct as long as $\psi_t > 1$, but ceases to be valid at a certain time t^* such that $\psi_t < 1$, which is given by $t^* = \lceil \tau \log \psi_0 \rceil$.

Next, we consider the case $\psi_0 < 1$. In this case the solution is given by $\psi_t = \psi_0 e^{-t/\tau} + \lambda(1 - e^{-t/\tau})$, which is always valid for $\lambda < 1$. Thus, when $\lambda < 1$ the system does not oscillate but it converges monotonically to a fixed point $\psi_\infty = \lambda$. However when $\lambda > 1$, this solution ceases to be valid at the time $t^* = \lceil \tau \log \frac{\lambda - \psi_0}{\lambda - 1} \rceil$ such that $\psi_t > 1$. Therefore, the solution ψ_t oscillates in time for $\lambda > 1$. For the case of $\psi_0 > 1$, the explicit solution is given by the general analytical expression which is plotted in Fig. 2G, right:

$$\begin{aligned} \psi_t &= \psi_0 e^{-t/\tau} && \text{for } t \in \left\{ 0, 1, \dots, t_1 = \lceil \tau \log \psi_0 \rceil \right\}, \\ \psi_t &= \psi_1 e^{-(t-t_1)/\tau} + \lambda \left(1 - e^{-(t-t_1)/\tau} \right) && \text{for } t \in \left\{ t_1, \dots, t_2 = t_1 + \left\lceil \tau \log \frac{\lambda - \psi_1}{\lambda - 1} \right\rceil \right\}, \\ \psi_t &= \psi_2 e^{-(t-t_2)/\tau} && \text{for } t \in \left\{ t_2, \dots, t_3 = t_2 + \lceil \tau \log \psi_2 \rceil \right\}. \end{aligned} \quad (6)$$

The general solution with initial condition $\psi(t_0) < 1$ can be written in a similar way.

Thus, the main condition for oscillations in the circuits is $\lambda > 1$, and if $\lambda < 1$, there is no oscillatory behavior, and the solution ψ_t converges monotonically to λ . Therefore,

the oscillatory phase is separated from the non-oscillatory phase by the condition:

$$\frac{\gamma_y}{k_y} = \left(\frac{\gamma_x}{\alpha}\right)^{-1}, \quad (7)$$

which is depicted in the phase diagram in Fig. 2G, left.

Thus, the repressor autoregulation at gene Y converts the circuit into a synchronized clock, a primary building block in any logic computational device. S1 File Section V and S2 File show all FFFs found across gene regulatory networks of the studied species spanning *A. thaliana*, *M. tuberculosis*, *B. subtilis*, *E. coli*, *salmonella*, *yeast*, mouse and humans. We also show in Table 1 the count of circuits across species and their associated Z-scores showing that these circuits are statistically significant. The algorithm to find these *fibers* in biological networks is explained in [24] and S1 File Section IV and it is available at <https://github.com/makselab/FiberCodes>.

Table 1. Symmetric circuits (*fibers*) count [24].

Species	Database	Nodes	Edges	AR Fiber			FFF			Fibonacci Fiber			n = 2 Fiber		
				N_{real}	$N_{\text{rand}} \pm SD$	Z-score	N_{real}	$N_{\text{rand}} \pm SD$	Z-score	N_{real}	$N_{\text{rand}} \pm SD$	Z-score	N_{real}	$N_{\text{rand}} \pm SD$	Z-score
Arabidopsis Thaliana	ATRM	790	1431	2	0.2 ± 0.5	4	2	0 ± 0	Inf	5	0.3 ± 0.6	8.1	0	N/A	N/A
Micobacterium tuberculosis	Research article	1624	3212	11	0.7 ± 0.8	13.2	6	0.2 ± 0.4	14.6	4	1.7 ± 1.4	1.7	0	N/A	N/A
Bacillus subtilis	SubtiWiki	1717	2609	35	0.3 ± 0.5	64.6	13	0.3 ± 0.5	23.4	1	1.3 ± 1.2	-0.2	2	0 ± 0	63.2
Escherichia coli	RegulonDB	879	1835	14	0.2 ± 0.5	29.1	12	0.1 ± 0.2	49.4	2	0.5 ± 0.8	1.9	1	0 ± 0	> 3
Salmonella SL1344	SalmoNet	1622	2852	21	0.7 ± 0.8	25	14	0.2 ± 0.4	32	2	1.4 ± 1.3	0.5	3	0 ± 0	> 3
Yeast				10			5			3			0		
	YTRP_regulatory	3192	10947	10	0.3 ± 0.6	17.3	4	0.2 ± 0.4	8.5	2	1.8 ± 1.3	0.2	0	N/A	N/A
	YTRP_binding	5123	38085	2	0.1 ± 0.3	6.3	0	N/A	N/A	0	N/A	N/A	0	N/A	N/A
Mouse	TRRUST	2456	7057	1	0.1 ± 0.4	2.3	0	N/A	N/A	6	0.3 ± 0.6	9.3	0	N/A	N/A
Human				1			1			100			1		
	TRRUST	2718	8215	0	N/A	N/A	0	N/A	N/A	10	0.4 ± 0.6	16.3	0	N/A	N/A
	TRRUST_2	2862	9396	0	N/A	N/A	0	N/A	N/A	11	0.4 ± 0.7	16	0	N/A	N/A
	KEGG	5164	59680	1	0.06 ± 0.25	3.76	1	0 ± 0	> 3	79	0.6 ± 0.7	112	1	0 ± 0	> 3

We report the Z-scores showing that all found fibers are statistically significant. We use a random null model with the same degree sequence (and sign of interaction) as the original network to calculate the random count N_{rand} and compare with the real circuit count N_{real} to get the Z-score.

A broad class of logic and dynamic repertoires in the class of fibers

The procedure to build more complex fibers can be systematically extended through an algebra of circuits that adds external regulators and loops to grow the *base* of symmetric circuits (Fig. 3 and S1 File Section IV A). In this space, the AR is the core loop unit referred to as $|n = 1, \ell = 0\rangle$ in the nomenclature of [24] since it has $n = 1$ loop and $\ell = 0$ external regulator (Fig. 3B), and the FFF is $|n = 1, \ell = 1\rangle$ (Fig. 3C).

From this starting point, one can grow the number of regulator genes, $|1, \ell\rangle$ with $\ell > 1$. This does not affect the complexity because all the relevant dynamics remain constrained to the sole loop in the FFF circuit. Likewise, there are a number of circuits that can correspond to $|1, 1\rangle$. However, only certain modifications conserve the topological class identified by $|1, 1\rangle$. For instance, changing the sign of the edges is allowed as long as the edges of each gene are the same, but removing the edge $X \rightarrow Z$ will break the symmetry of the fiber, so it is not allowed. Adding a second node downstream of Y will conserve the topological class but only if it interacts with X. This situation changes as soon as the *fiber* feeds information back to the external world. This is the case of the circuits in Fig. 3D, where the gene Y now regulates its own regulator gene X. The inclusion of this second feedback loop results in the coexistence of two time-scales in the network. This, in turn, increases the diversity of trajectories and delays in the network; a dynamic complexity that is measured by the divergence of the input tree, which is captured by the sequence Q_t representing the number of source genes with

paths of length $t - 1$ to the target gene, see Fig. 3 and [24]. Simply put, the input tree is a rooted tree with a gene at the root ($Q_1 = 1$), and Q_t represents the number of genes in the t -th layer of the input tree. Then, the divergence of the input tree is captured by its branching ratio measured by $n = \left(\frac{Q_{t+1}}{Q_t}\right)_{t \rightarrow \infty}$, see [24] for details.

A quantitative analysis of this measure yields exactly the golden ratio $\left(\frac{Q_{t+1}}{Q_t}\right)_{t \rightarrow \infty} = \varphi = (1 + \sqrt{5})/2 = 1.6180\dots$ for the circuits in Fig. 3D, revealing that the input tree is a Fibonacci sequence $Q_t = Q_{t-1} + Q_{t-2}$ updating the current state two steps backwards, see [24]. We have called this class of circuits, Fibonacci Fibers, in [24]. For example, the repressor interactions between genes $X = uxuR$, $Y = exuR$, and $Z = lgoR$ from the *E. coli* network function exactly as a Fibonacci Fiber (Fig. 3D). Other typical examples of Fibonacci Fibers in the transcriptional networks across species are also shown in Fig. 3D. S1 File Section V and S2 File show all found *fibers*, and Table 1 the counts for all *fibers* and their associated Z-scores showing that these circuits are statistically significant. The important component of these circuits is the delay in the feedback loop through the regulator from $Y \rightarrow X$ and back to Y captured by the Q_{t-2} term in the Fibonacci sequence. This circuit has been synthetically implemented by Stricker *et al.* [22] using a hybrid promoter that drives the transcription of genes *araC* and *lacI* forming a dual-feedback circuit. The functionality of this circuit has been demonstrated to be robust oscillations due to the negative feedback loop [22]. We will show next that a symmetry breaking in this Fibonacci circuit forms the *base* of the JK flip-flop, which is the universal storage device of computer memories [33].

The complexity of the Fibonacci Fiber with feedback to the regulator is $1.6180\dots$, which is lower than the number of loops in the circuit (two). The intuition of what this reveals is that, in this circuit the regulator X is still not part of the *base* (see Fig. 3D), since it does not receive input from itself and hence it is not within the symmetry of the *fiber*. This, in turn, indicates naturally that the next element in the hierarchy of *fibers* results from the inclusion of an AR loop in X . This creates a fully symmetric circuit (Fig. 3E) with a core $|2, \ell = 0\rangle$ that feeds the reporter/enzyme Z . In this case, the complexity of the circuit is exactly two (the number of autoregulators within the *fiber*). Examples are shown in Fig. 3E and Supplementary Materials.

Broken symmetry circuits as memory storage devices

All symmetric circuits shown in Fig. 3 [24] work as clocks with varying levels of sophistication and robustness given by their time-scales or loops (see S1 File Sections III C and IV A). Additionally, the more complex Fibonacci Fibers store memory dynamically by integrating sequences of its two immediate past states, according to the input tree, which computes temporal convolutions. However, this is only a short-term memory, stored dynamically and continually erased. This raises the necessity of understanding how these canonical biological circuits can perform controlled memory set and reset, a fundamental component of all computing devices [33].

We show next that static memory storage requires breaking the fibration symmetry of each circuit creating structures analogous to ‘flip-flops’ [33] in electronics that use a bistable toggle switch [14, 15] to store a bit of binary information into computer memory. As we show below, in genetic networks, symmetry breaking endows the circuits with the ability to remember.

Next, we extend the constructive process described above to include symmetry breaking. We do so by mimicking an evolutionary process where circuits ‘grow’ by a ‘duplication’ event (analogous to gene duplication in evolution) that conserves the *base* of the original circuit (Fig. 4, first and second row). Then, breaking the symmetry creates a new functionality. We begin this with the simplest case of AR gene Y : $|n = 1, \ell = 0\rangle$. This gene is duplicated by ‘opening up’ the AR loop into two mutually

repressed replica genes, Y and Y' (Fig. 4, second row). This creates a bistable toggle switch as studied in synthetic genetic circuits [14,15] that is topologically equivalent to the core AR loop [1,0] since both have the same input tree and *base* (Fig. 4, first row).

The symmetry of the replica circuit is then explicitly broken by including different inputs, S and R, to regulate genes Y and Y', respectively (Fig. 4, third row). S and R represent either genes or effectors that break the symmetry of the circuit. Symmetry is now broken, and the genetic circuit becomes analogous to a Set-Reset (SR) flip-flop [33], the simplest canonical circuit to store a bit of binary information in electronic computer memory (see Fig. 4, fourth row).

The symmetry is explicitly broken by applying set-reset inputs $S \neq R$. Specifically, when $S = 1$ and $R = 0$, the circuit stores a bit of information. But here is the interesting fact: this state is kept in memory even when $S = R = 1$. That is, the circuit remains in the broken symmetry state even if the inputs are now equal and symmetric. In other words, the symmetry is now 'spontaneously' broken [34], since a specific state is selected even without external bias, thus allowing the circuit to remember its state.

Thus, this genetic network is a toggle switch as studied in synthetic genetic circuits [14,15] analogous to the SR flip-flop logic circuit shown in Fig. 4, fourth row. When the controlling inputs are $S = 0$ and $R = 1$, the SR flip-flop stores one bit of information resulting in $Q = 1$ and $\bar{Q} = 0$ ($\bar{Q} = \text{not } Q$, and the output Q is the logic conversion of **not** Y). The SR flip-flop retains this logical state even when the controlling inputs change. In other words, when $S = 1$ and $R = 1$, the feedback (the repressor interactions between Y and Y') maintains the outputs Q and \bar{Q} to its previous state. This state changes only when we reset the circuits with $S = 1$ and $R = 0$. In this last case, the SR flip-flop stores $Q = 0$ and $\bar{Q} = 1$, which is also remembered when both inputs are high ($S = 1$ and $R = 1$, S1 File Section IV B).

This spontaneous symmetry breaking [34] has analogy with a ferromagnetic material. When the temperature is high enough, the ferromagnet does not show any magnetic property. Moreover, even lowering the temperature, in absence of any polarizing field, the material does not magnetize. On the contrary, if an external magnetic field is applied to the ferromagnet, like a magnet put in contact to a needle for enough time, and then removed, then the needle becomes magnetic itself, in that it remembers the direction of the previously applied magnetic field, thus breaking, spontaneously, the rotational symmetry. Biological realizations of this replica symmetry breaking process are shown in Fig. 4, last row. Full list of symmetry broken circuits in gene regulatory networks across species appears in S1 File Section V and S2 File. Table 2 shows the Z-scores of these circuits indicating their significance. The algorithm to identify these broken symmetry flip-flops in biological networks is developed in S1 File Section VII and is available at <https://github.com/makselab/CircuitFinder>.

Table 2. Broken symmetry circuits count.

Species	Database	Nodes	Edges	SR flip-flop			Clocked SR flip-flop			JK flip-flop		
				N_{real}	$N_{\text{rand}} \pm SD$	Z-score	N_{real}	$N_{\text{rand}} \pm SD$	Z-score	N_{real}	$N_{\text{rand}} \pm SD$	Z-score
Arabidopsis Thaliana	ATRM	790	1431	47	1.6 ± 1.2	36.40	3	0.2 ± 0.5	5.80	2	0 ± 0	> 3
Micobacterium tuberculosis	Research article	1624	3212	6	1.7 ± 1.4	3.20	0	N/A	N/A	0	N/A	N/A
Bacillus subtilis	SubtiWiki	1717	2609	3	2.1 ± 1.4	0.6	0	N/A	N/A	0	N/A	N/A
Escherichia coli	RegulonDB	879	1835	14	2.1 ± 1.4	8.40	3	0.3 ± 0.8	3.30	0	N/A	N/A
Salmonella SL1344	SalmoNet	1622	2852	6	1.4 ± 1.2	3.80	0	N/A	N/A	0	N/A	N/A
Yeast					27			58			1	
	YTRP_regulatory	3192	10947	9	5 ± 2.5	1.60	3	3 ± 3.6	0	0	N/A	N/A
	YTRP_binding	5123	38085	31	21.6 ± 5.8	1.60	192	103.3 ± 45.6	1.90	2	6.8 ± 6.1	-0.8
Mouse	TRRUST	2456	7057	82	4 ± 2.1	37.70	216	1.9 ± 2.7	79.50	25	0.004 ± 0.06	417
Human					192			566			90	
	TRRUST	2718	8215	89	4.3 ± 2.1	40.50	247	3.5 ± 4.8	50.60	45	0.02 ± 0.2	225
	TRRUST.2	2862	9396	103	5 ± 2.3	43	319	5.9 ± 7.2	43.20	45	0.02 ± 0.3	150

We report the corresponding Z-score statistics as computed in Table 1.

Extending this duplication and symmetry breaking process to the FFF (Fig. 4, second column), one can replicate the X and Y genes from the FFF *base* to create a circuit isomorphic to the Clocked SR flip-flop, another computer memory building block [33] (see S1 File Section IV B). The symmetry is broken by regulators or inducers of genes X and X' acting as S (set) and R (reset) of memory, and it is restored when $S = R$, leaving the system 'magnetized'. The hierarchy continues by replicating the Fibonacci Fiber and consequent breaking of symmetry when the inputs J and K are different (Fig. 4 third column, see S1 File Section IV B). This structure is isomorphic (i.e., has the same *base*) to the JK flip-flop in electronics, which is the most widely used of all flip-flop designs [33]. In its symmetric state, the JK flip-flop is isomorphic to the symmetric Fibonacci *base*. In the symmetry broken phase, it acts as a memory device which presents two possibilities. A 'chiral' symmetry (where Y feeds X and Y' feeds X') and a 'parity' symmetry (left-right reflection, where Y feeds X' and Y' feeds X). This last one is the one realized in biological circuits, see Fig. 4, third column. Examples of JK flip-flops are abundant in gene regulatory networks in human and mouse. They are shown in Fig. 4, last row and full list in S1 File Section V, S2 File, and Z-scores in Table 2.

Discussion

In summary, fibration symmetries and broken symmetries in gene regulatory networks reveal the functions of synchronization, clocks and memory through electronic analogues of transistors, ring oscillators, current-mirror circuits, and flip-flops. They result in a hierarchy of building blocks with progressively more complex dynamics obtained by iterating a procedure of replication and symmetry breaking. Beyond the circuits discussed here, the biological hierarchy can be extended to any number m of loops of length d and autoregulators in the *fiber* n , to form ever more sophisticated circuits whose complexity is expressed in generalized Fibonacci sequences $Q_t = nQ_{t-1} + mQ_{t-d}$.

Gene regulatory structures are a mixture of combinational logic circuits, like FFF, and sequential logic circuits, like FF. They provide the network with a structure analogous to a programmable logic device or chip where the 'register' is a set of flip-flop circuits tied up together acting as the memory clock of the genetic network that feeds the combinatorial logic circuits made of simpler feed-forward circuit of low symmetry. Complex biological circuitry can then be seen as an emergent process guided by the laws of symmetry that determine biological functions analogous to electronic components. The discovery of these building blocks and building rules of logic computation will allow to: (1) systematically design synthetic genetic circuits following biological symmetry, and (2) systematically map the structure and function of all biological networks, from the symmetries of the connectome [35] to genetic [24], protein and metabolic networks, following a first principle theoretical approach.

Supporting information

S1 File. Supplementary Materials. Detailed description of all analytical solutions mentioned in the main text, of the data acquisition and treatment, and detailed description of the proposed algorithm to find fibers.

S2 File. List of symmetry and broken symmetry circuits. In S2 File we present a list of circuits found in different species.

Acknowledgments

351

We are grateful to L. Parra and W. Liebermeister for discussions.

352

References

1. Hartwell LH, Hopfield JJ, Leibler S, Murray AW. From molecular to modular cell biology. *Nature*. 1999;402: C47-C52.
2. Milo R, Shen-Orr SS, Itzkovitz S, Kashtan N, Chklovskii D, Alon U. Network motifs: simple building blocks of complex networks. *Science*. 2002;298: 824-827.
3. Shen-Orr SS, Milo R, Mangan S, Alon U. Network motifs in the transcriptional regulation network of *Escherichia coli*. *Nature Genet*. 2002;31: 64-68.
4. Alon U. *An Introduction to Systems Biology: Design Principles of Biological Circuits*. Boca Raton: CRC Press; 2006.
5. Klipp E, Liebermeister W, Wierling C, Kowald A, Herwig R. *Systems Biology: a textbook*. Weinheim: Wiley-VCH; 2016.
6. Ingram PJ, Stumpf MP, Stark J. Network motifs: structure does not determine function. *BMC Genomic*. 2006;7: 108.
7. Payne JL, Wagner A. Function does not follow form in gene regulatory circuits. *Sci Rep*. 2015;5: 13015.
8. Macía J, Widder S, Solé R. Specialized or flexible feed-forward loop motifs: a question of topology. *BMC Syst Biol*. 2009;3: 84.
9. Ahnert SE, Fink TMA. Form and function in gene regulatory networks: the structure of network motifs determines fundamental properties of their dynamical state space. *J Royal Soc Interface*. 2016;13: 20160179.
10. Tyson JJ, Chen KC, Novak B. Sniffers, buzzers, toggles and blinkers: dynamics of regulatory and signaling pathways in the cell. *Curr Opin Cell Biol*. 2003;15(2): 221-31.
11. Monod J, Jacob F. General conclusions: teleonomic mechanisms in cellular metabolism, growth and differentiation. *Cold Spring Harb Symp Quant Biol*. 1961;26: 389-401.
12. Teo JY, Woo SS, Sarpeshkar R. Synthetic Biology: A Unifying View and Review Using Analog Circuits. *IEEE Trans. on Biomed. Circuits and Syst*. 2015;9: 453-474.
13. Dalchau N, Szé G, Hernansaiz-Ballesteros R, Barnes CP, Cardelli L, Phillips A, et al. Computing with biological switches and clocks. *Natural Computing*. 2018;17: 761-779.
14. Atkinson MR, Savageau MA, Myers JT, Ninfa AJ. Development of genetic circuitry exhibiting toggle switch or oscillatory behavior in *Escherichia coli*. *Cell*. 2003;113: 597-607.
15. Gardner TS, Cantor CR, Collins JJ. Construction of a genetic toggle switch in *Escherichia coli*. *Nature*. 2000;403: 339-342.

16. Kramer BP, Fussenegger M. Hysteresis in a synthetic mammalian gene network. *Proc Natl Acad Sci USA*. 2005;102: 9517-9522.
17. Kramer BP, Viretta AU, Baba MD-E, Aube D, Weber W, Fussenegger M. An engineered epigenetic transgene switch in mammalian cells. *Nature Biotech*. 2004;22: 867-870.
18. Guet CC, Elowitz MB, Hsing W, Leibler S. Combinatorial synthesis of genetic networks. *Science*. 2002;296: 1466-1470.
19. Ajo-Franklin CM, Drubin DA, Eskin JA, Gee EP, Landgraf D, Phillips I, et al. Rational design of memory in eukaryotic cells. *Genes Dev*. 2007;21: 2271-2276.
20. Ham TS, Lee SK, Keasling JD, Arkin AP. Design and construction of a double inversion recombination switch for heritable sequential genetic memory. *PLoS One*. 2008;3: e2815.
21. Elowitz MB, Leibler S. A synthetic oscillatory network of transcriptional regulators. *Nature*. 2000;403: 335-338.
22. Stricker J, Cookson S, Bennett MR, Mather WH, Tsimring LS, Hasty J. A fast, robust and tunable synthetic gene oscillator. *Nature*. 2008;456: 516-519.
23. Tigges M, Marquez-Lago TT, Stelling J, Fussenegger M. A tunable synthetic mammalian oscillator. *Nature*. 2009;457: 309-312.
24. Morone F, Leifer I, Makse HA. Fibration symmetries uncover the building blocks of biological networks. *Proc Natl Acad Sci USA*. 2020;117: 8306-8314.
25. Mangan S, Alon U. Structure and function of the feed-forward loop network motif. *Proc Natl Acad Sci USA*. 2003;100: 11980-11985.
26. Mangan S, Zaslaver A, Alon U. The coherent feedforward loop serves as a sign-sensitive delay element in transcription networks. *J Mol Biol*. 2003;334: 197-204.
27. Glass L, Kauffman SA. The logical analysis of continuous, non-linear biochemical control networks. *J Theor Biol*. 1973;38: 103-129.
28. Mangan S, Zaslaver A, Alon U. Negative autoregulation increases the input dynamic-range of the arabinose system of *Escherichia coli*. *BMC Sys Biol*. 2011;5: 111.
29. Golubitsky M, Stewart I. Nonlinear dynamics of networks: the groupoid formalism. *Bull Am Math Soc*. 2006;43: 305-364.
30. Boldi P, Vigna S. Fibrations of graphs. *Discrete Mathematics*. 2001;243: 21-66.
31. Anderson PW. The concept of frustration in spin glasses. *J of the Less-Common Metals*. 1978;62: 291-294.
32. Widlar RJ. Some circuit design techniques for linear integrated circuits. *IEEE Trans Circuit Theory*. 1965;4: 586-590. See also Widlar RJ: US Patent Number 3,320,439; Filed May 26, 1965; Granted May 16, 1967: Low-value current source for integrated circuits and Widlar RJ. Design techniques for monolithic operational amplifiers. *IEEE Solid-State Circuits*. 1969;4: 184-191.
33. Horowitz P, Hill W. *The Arts of Electronics*. 3rd ed. New York:Cambridge University Press; 2015.

34. Weinberg S. The Quantum Theory of Fields. Cambridge: Cambridge University Press; 2005.
35. Morone F, Makse HA. Symmetry group factorization reveals the structure-function relation in the *Caenorhabditis elegans* connectome. Nat Commun. 2019;10: 4961.

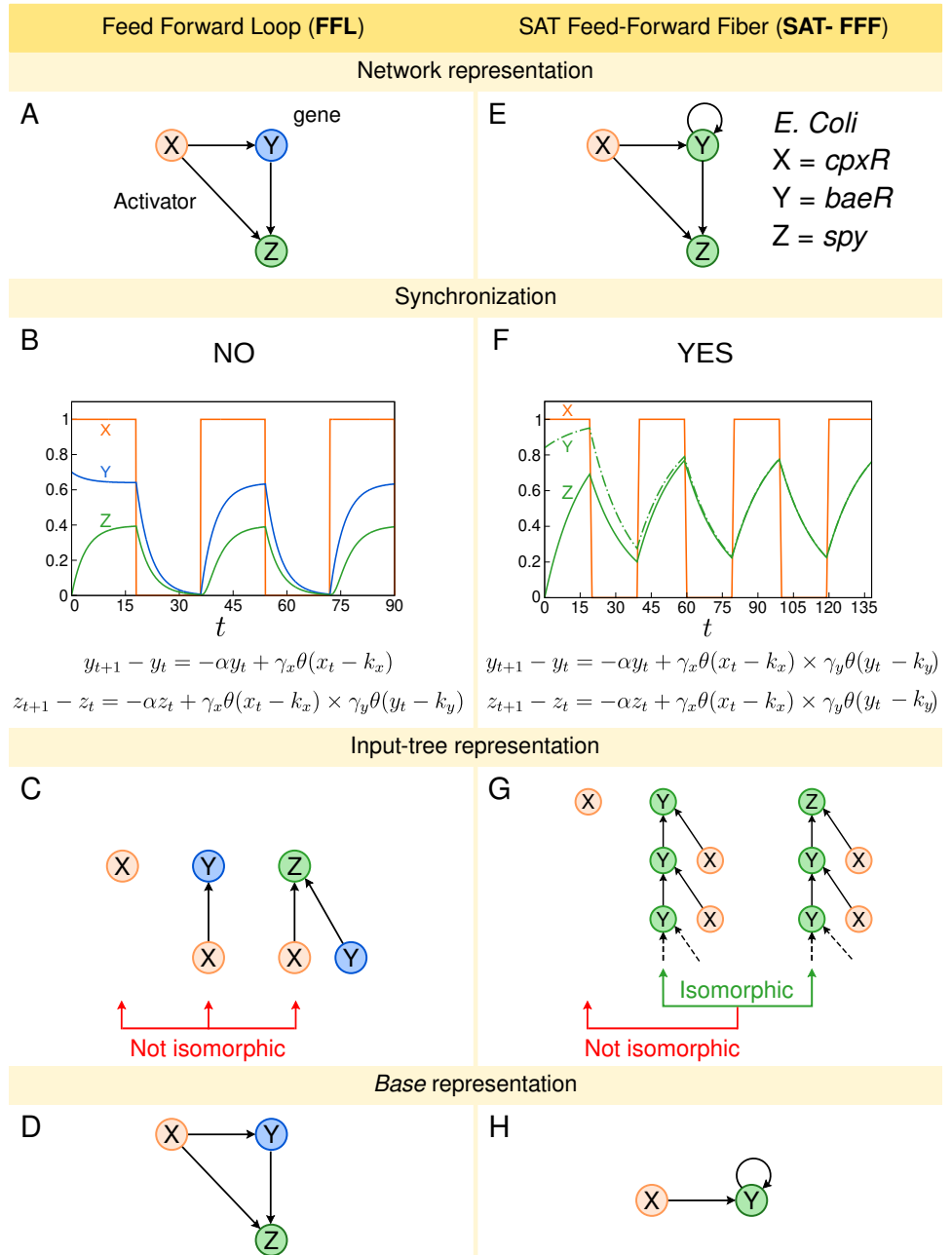


Fig 1. Feed-Forward Loop (FFL) and Feed-Forward Fiber (FFF). A: FFL network representation. B: Numerical solution of FFL dynamics. The expression levels of genes Y and Z do not synchronize. The oscillation pattern presented is due to the square-wave behavior of gene X expression levels. We use $\alpha = 2.0$, $\gamma_x = 0.12$, $\gamma_y = 0.7$, $k_x = 0.5$, $k_y = 0.1$, $y_0 = 0.7$ and $z_0 = 0.0$. C: Input tree representation of FFL. The input trees of genes X, Y, and Z are not isomorphic, as a consequence, their expression levels do not synchronize. D: Base representation of FFL. The *base* is the same as the original circuits since there are no symmetries. E: SAT-FFF network representation. As an example, we consider genes *cpxR* = X, *baeR* = Y, and *spy* = Z from the gene regulatory network of *E. coli*. The addition of the autoregulation leads to a symmetry between the expression levels of genes Y and Z. F: The numerical solution of the SAT-FFF dynamics shows the synchronization of the expression levels of genes Y and Z. We use $\alpha = 0.06$, $\gamma_x = 0.775$, $\gamma_y = 0.775$, $k_x = 0.5$, $k_y = 0.1$, $y_0 = 0.85$ and $z_0 = 0.0$. Again, the oscillation is due to the wave-like pattern of X. G: As a result, genes Y and Z have isomorphic input trees. However, the input tree of the external regulator *cpxR* is not isomorphic, despite the fact that it directly regulates the *fiber*. H: Since Y and Z synchronize, gene Z can be collapsed into Y, resulting in a simpler *base* representation.

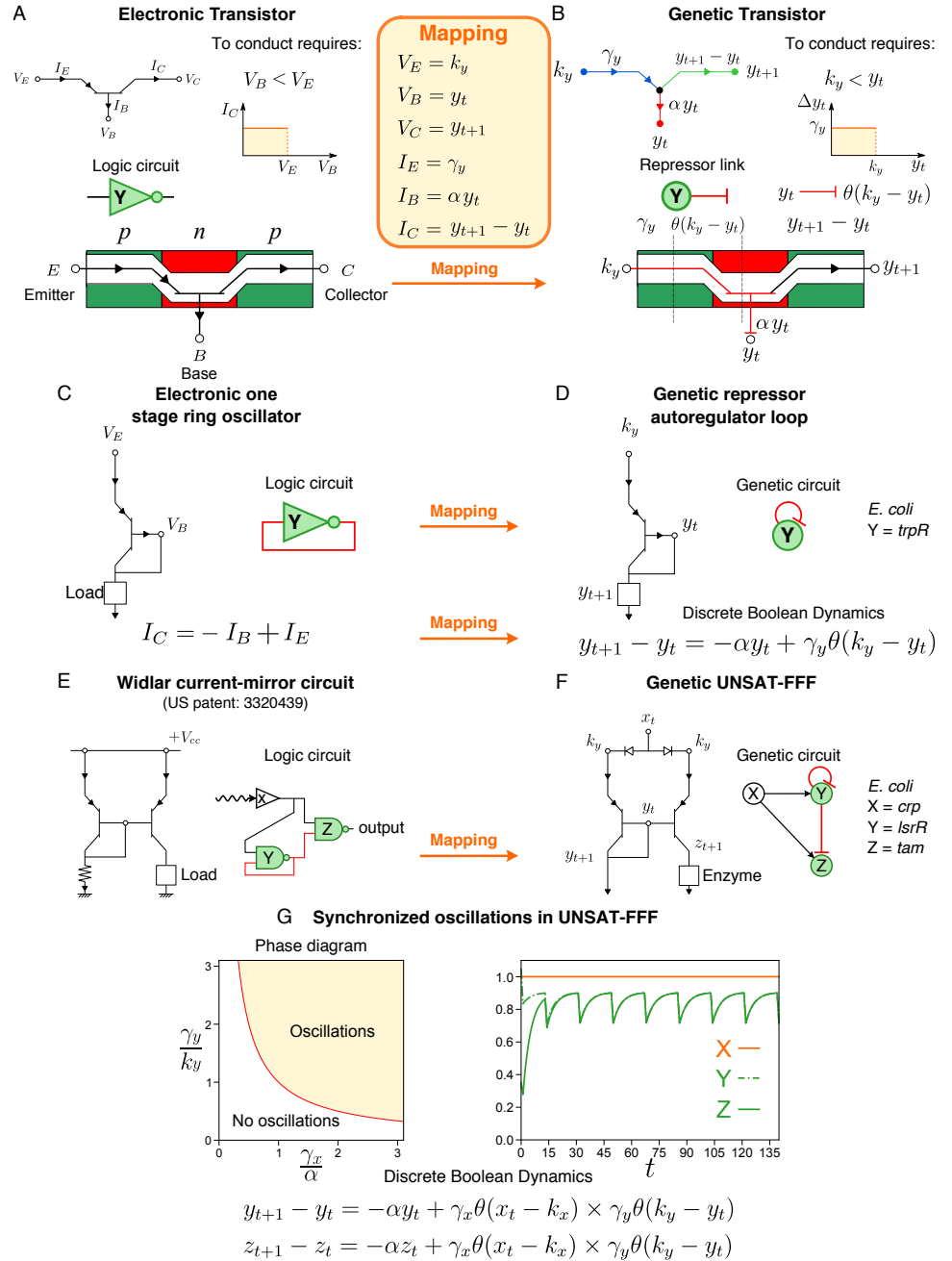


Fig 2. Mapping between electronic and biological transistor. A: A pnp transistor allows current flow if the voltage applied to its base is lower than the voltage at its emitter ($V_B < V_E$). Since it has a high (low) output for a lower (high) input, it is logically represented by a NOT gate. The yellow box shows the mapping between the pnp transistor and the biological repressor. B: A repressor regulation link plays the role of the pnp transistor since the rate of expression of a gene is repressed by gene Y if $k_y < y_t$. C: By connecting the base of the transistor to its collector, one forms a one stage ring oscillator. D: This connection is translated to the biological analogue as a repressor autoregulation at gene Y. In this way, the rate expression of gene Y is able to oscillate, depending on the adjustment of parameters α , k_y and γ_y (see S1 File Section III). E: Widlar current-mirror circuit and F: its biological analogue (UNSAT-FFF). By mirroring the ring oscillator, the Widlar mirror circuit allows synchronization and oscillations (see S1 File Section III). G: Phase diagram of oscillations of the UNSAT-FFF. An oscillatory phase is defined by the condition $\gamma_y/k_y > (\gamma_x/\alpha)^{-1}$ (see S1 File Section III). For instance, on the right side, we plot the solution of the discrete dynamics for a set of parameters satisfying such condition. Specifically, $\alpha = 0.205$, $\gamma_x = 0.454$, $\gamma_y = 0.454$, $k_x = 0.5$, and $k_y = 1.0$.

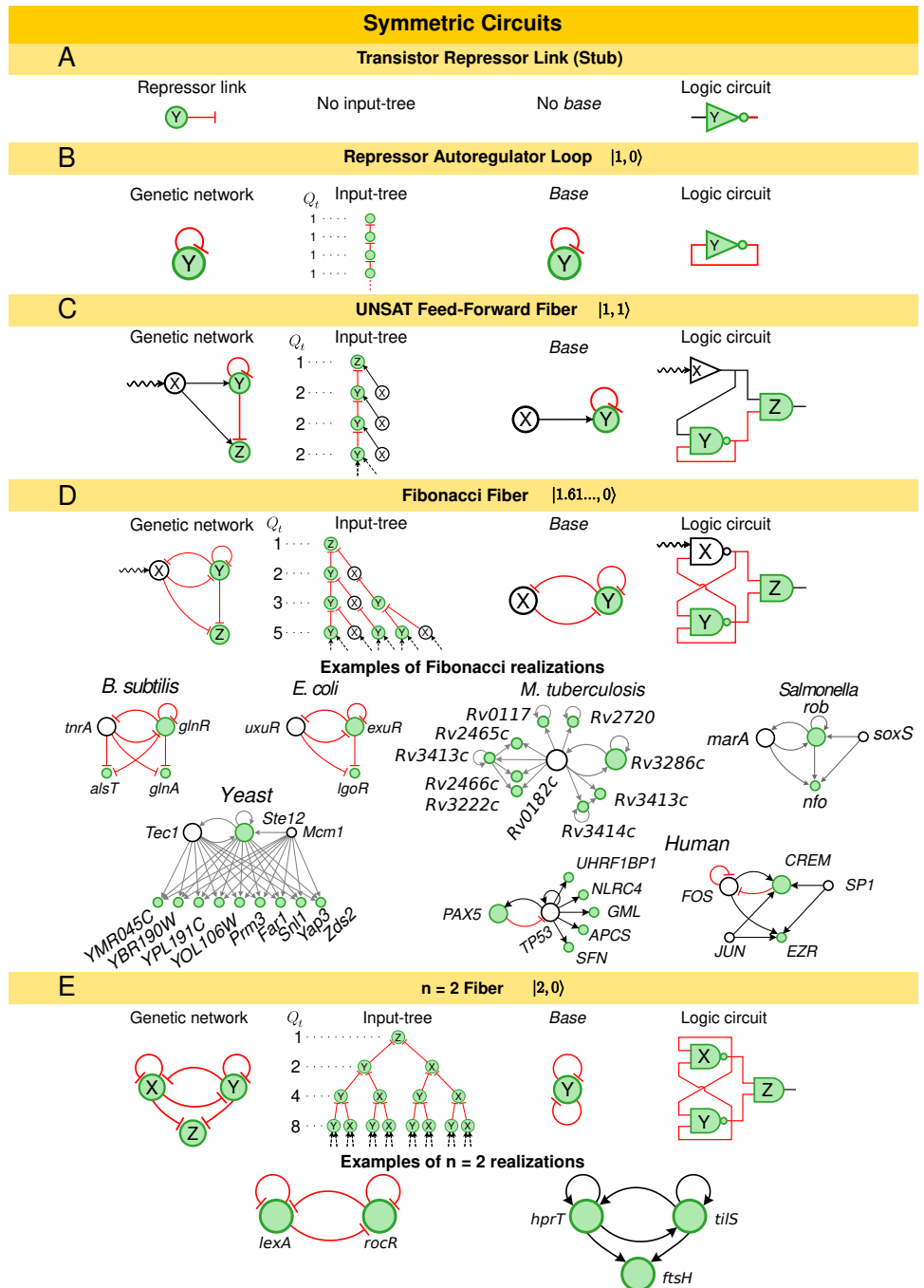


Fig 3. Symmetric circuits [24] function as clocks. The addition of autoregulation loops and feedback loops results in a hierarchy of circuits of increasing complexity. For example, turning the A: repressor link into a B: repressor autoregulation results on an input tree that feeds its own expression levels with $Q_t = 1$ and branching ratio $n = 1$ and it is equivalent to its own *base*. C: The addition of an external regulator ($\ell = 1$) creates the UNSAT-FFF where genes Y and Z synchronize and oscillate. This can be verified in its corresponding input tree and logic circuit. D: The addition of a second feedback loop results in an input tree that follows the Fibonacci sequence $Q_t = 1, 2, 3, 5, 8, \dots$. Here, gene X is not part of the *base*. The branching structure of the input tree implies that the Fibonacci Fiber can oscillate and synchronize, but is unable to store static information. Examples are shown from all studied species. E: The second autoregulation at X results in a symmetric input tree with $Q_t = 2Q_{t-1}$ and branching ratio $n = 2$. This *fiber* collapses into a *base* with two autoregulators. Examples of $n = 2$ Fiber are two *fibers* from the regulatory networks of *B. subtilis*. In this figure, we present activator links (black), repressor links (red), and interactions with unknown functionality (grey).

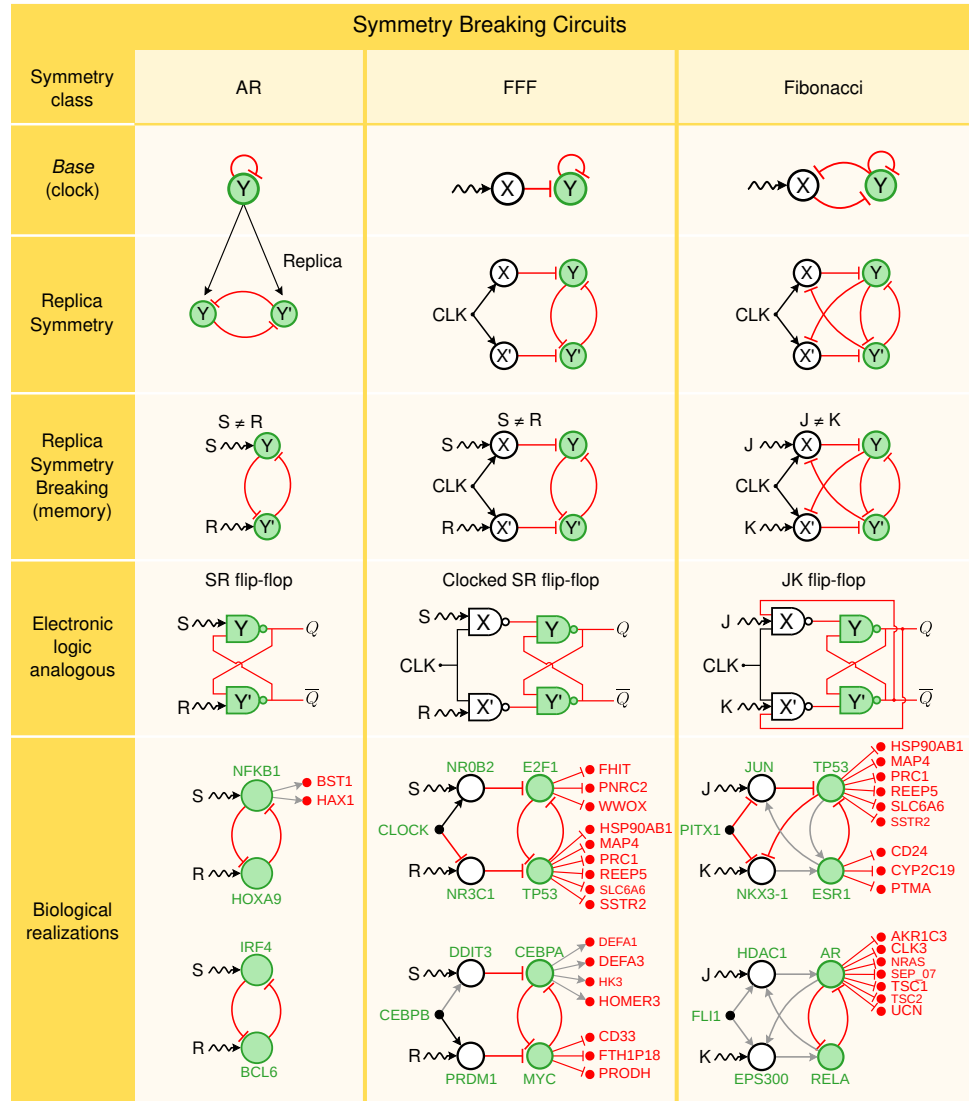


Fig 4. Broken symmetry circuits function as memory. AR (first column): The replica symmetry duplication of the AR symmetric circuit results in a network that is analogous to the SR flip-flop circuit. The symmetry between Y and Y' is broken by the inputs S and R , such that $S \neq R$, resulting into a pair logical outputs Q and $\bar{Q} = \text{not}(Q)$. **FFF (second column):** Following the same strategy, we replicate the FFF through a replica symmetry duplication. Note that this operation adds a second level of logic gates to the SR flip-flop. In order to have consistent logic operations, we add an input clock gene CLK in addition to S and R . The resulting circuit is analogous to the Clocked SR flip-flop logic circuit. **Fibonacci (third column):** The replica symmetry duplication of the Fibonacci Fiber results in a logic circuit which is analogous to the JK flip-flop. For each symmetry breaking class, we show two examples of circuits from the human regulatory network. The external regulator genes, S and R (J and K), provide inputs which are logically processed by the circuit, accordingly to the type of interaction links between the genes, activators (black arrows) or repressors (red flat links). The outputs of the circuits (green genes) regulate the expression levels of other genes (in red) without affecting the circuit functionality. Here, grey arrows correspond to interactions with unknown functionality.

Supplementary Materials:

Circuits with broken fibration symmetries perform core logic computations in biological networks

Ian Leifer, Flaviano Morone, Saulo D. S. Reis, José S. Andrade Jr., Mariano Sigman, and Hernán A. Makse

CONTENTS

I. Feed-forward loop: FFL	3
A. FFL discrete time model	3
B. FFL ODE	4
C. FFL with OR gate	6
II. Satisfied Feed-Forward Fiber: SAT-FFF	7
A. SAT-FFF discrete time model	7
B. SAT-FFF ODE	9
III. Unsatisfied Feed-Forward Fiber: UNSAT-FFF	11
A. UNSAT-FFF ODE	11
B. Period-amplitude relationship	14
C. UNSAT-FFF clock functionality	16
IV. Examples of symmetry and broken symmetry circuits	17
A. Symmetry circuits (<i>fibers</i>) from [24]	17
1. Repressor regulator link (stub)	17
2. Repressor AR loop: $ 1, 0\rangle$	17
3. UNSAT-FFF: $ 1, 1\rangle$	17
4. Fibonacci Fiber: $ 1.6180\dots, 0\rangle$	18
5. $n = 2$ Fiber: $ 2, 0\rangle$	18
B. Symmetry breaking circuits	19
1. AR symmetry breaking circuit: SR flip-flop	19
2. FFF symmetry breaking circuit: Clocked SR flip-flop	20
3. Fibonacci symmetry breaking circuit: JK flip-flop	20
V. Description of datasets	21

arXiv:2006.13334v1 [q-bio.GN] 23 Jun 2020

VI. Algorithm to find fibers	21
VII. Algorithm to find broken symmetry circuits	24
References	27

I. FEED-FORWARD LOOP: FFL

In what follows, we analyze in detail the FFL. First, we present the analytical solution for the discrete time model of the FFL, where we show that the FFL does not synchronize nor oscillates. After that, we reach the same conclusion by using a continuous variable approach. Finally, we show the discrete time solution with the OR gate. Solutions for the FFL have been considered in the literature. Here we adapt those results to the particular models used in our studies to perform consistent comparisons with the solutions of the fiber dynamics obtained through the paper.

A. FFL discrete time model

Starting from Eq. (1) in the main text, we define rescaled variables $\psi_t = y_t/k_y$ and $\zeta_t = z_t/k_y$, we rewrite Eq. (1) as

$$\begin{aligned}\psi_{t+1} &= \beta\psi_t + \alpha\eta\theta(x_t - k_x), \\ \zeta_{t+1} &= \beta\zeta_t + \alpha\lambda\theta(x_t - k_x)\theta(\psi_t - 1),\end{aligned}\tag{1}$$

where we set $\beta = (1 - \alpha)$, $\eta = \gamma_x/\alpha k_y$, and $\lambda = \gamma_x\gamma_y/\alpha k_y$. Equation (1) defines an iterative map $\psi_{t+1} = f(\psi_t)$ which provides a solution

$$\psi_t = f(\psi_{t-1}) = f^2(\psi_{t-2}) = \dots = f^t(\psi_0).\tag{2}$$

A closed form for ψ_t depends on the value of x . For the sake of simplicity, consider $x_t = x$ constant in time. If $x < k_x$, the solution is simple, and always decays as $\psi_t = \psi_0 e^{-t/\tau}$, where we choose to write $\beta^t = e^{-t/\tau}$ such as $\tau^{-1} = -\log(1 - \alpha)$. On the other hand, if $x > k_x$, the iterative map is $f(\psi_t) = \beta\psi_t + \eta$, leading to a solution that converges to η as $\psi_t = \psi_0 e^{-t/\tau} + \eta(1 - e^{-t/\tau})$. Therefore, the solution to ψ_t is given by:

$$\psi_t = \psi_0 e^{-t/\tau} + \eta(1 - e^{-t/\tau})\theta(x_t - k_x).\tag{3}$$

Similarly, the solution for ζ_t depends on x , but it also depends on ψ_0 and η . For $x < k_x$, it always decays to zero as $\zeta_t = \zeta_0 e^{-t/\tau}$. When $x > k_x$, the variable ζ_t follows different behaviors.

For $\psi_0 < 1$, we also find a solution that decays as $\zeta_t = \zeta_0 e^{-t/\tau}$. However, if $\eta > 1$, this solution ceases to be valid at a given time t^* such that $\psi_{t^*} > 1$, which is given by $t^* = \lceil \tau \log((\eta - \psi_0)/(\eta - 1)) \rceil$. Here, $\lceil x \rceil$ denotes the smallest integer larger than x , e.g., $\lceil 1.5 \rceil = 2$. For $t > t^*$, as ψ_t saturates to η , the rescaled variable ζ_t converges to λ as $\zeta_t = \zeta_0 e^{-(t-t^*)/\tau} + \lambda (1 - e^{-(t-t^*)/\tau})$.

Next, we consider the case $\psi_0 > 1$. In this case, the solution for ζ_t is given by $\zeta_t = \zeta_0 e^{-t/\tau} + \lambda(1 - e^{-t/\tau})$, for $\eta > 1$. In contrast, when $\eta < 1$, this solution is valid only up to $t^* = \lceil \tau \log((\psi_0 - \eta)/(1 - \eta)) \rceil$, such that $\psi_t < 1$. As ψ_t saturates to η , the rescaled variable ζ_t exponentially decays as $\zeta_t = \zeta_0 e^{-(t-t^*)/\tau}$.

To summarize, the possible solutions for ζ_t depending on ψ_0 and η are:

$$\begin{aligned}
\psi_0 > 1, \eta > 1 &\rightarrow \zeta_t = \zeta_0 e^{-t/\tau} + \lambda(1 - e^{-t/\tau}), \\
\psi_0 > 1, \eta < 1 &\rightarrow \zeta_t = \zeta_0 e^{-t/\tau} + \lambda(1 - e^{-t/\tau}) \quad \text{for } t \in \left\{0, 1, \dots, t_1 = \left\lceil \tau \log \frac{\psi_0 - \eta}{1 - \eta} \right\rceil\right\}, \\
&\quad \zeta_t = \zeta_1 e^{-(t-t_1)/\tau} \quad \text{for } t > t_1, \\
\psi_0 < 1, \eta > 1 &\rightarrow \zeta_t = \zeta_0 e^{-t/\tau} \quad \text{for } t \in \left\{0, 1, \dots, t_1 = \left\lceil \tau \log \frac{\eta - \psi_0}{\eta - 1} \right\rceil\right\}, \\
&\quad \zeta_t = \zeta_1 e^{-(t-t_1)/\tau} + \lambda(1 - e^{-(t-t_1)/\tau}) \quad \text{for } t > t_1, \\
\psi_0 < 1, \eta < 1 &\rightarrow \zeta_t = \zeta_0 e^{-t/\tau}.
\end{aligned} \tag{4}$$

Here, $\zeta_1 = \zeta_{t=t_1}$.

From this discussion, we find that the rescaled variables ψ_t and ζ_t do not synchronize. That is, they do not reach the same value at their fixed points: $\psi_t \neq \zeta_t$ when $t \rightarrow \infty$, unless we use a specific set of parameters. Moreover, ψ_t and ζ_t also do not reach oscillatory states. The same conclusion is extended to the original variables y_t and z_t .

B. FFL ODE

In order to show that our results presented in the main text are consistent with a continuous variable approach, now we focus our attention on the modelling of the FFL [4, 20, 21] by using ordinary differential equations (ODE). First, we write the ODE governing the

dynamics of expression levels $y(t)$ and $z(t)$:

$$\begin{aligned}\dot{y}(t) &= -\alpha y(t) + \gamma_x \theta(x(t) - k_x), \\ \dot{z}(t) &= -\alpha z(t) + \gamma_x \theta(x(t) - k_x) \times \gamma_y \theta(y(t) - k_y).\end{aligned}\tag{5}$$

For the sake of simplicity, we consider $x(t) = x$ constant in time.

By using the rescaled functions $\psi(t) = y(t)/k_y$ and $\zeta(t) = z(t)/k_y$, we rewrite Eq. (5) as the following set of ODEs:

$$\begin{aligned}\dot{\psi}(t) + \alpha\psi(t) &= \alpha\eta\theta(x_t - k_x), \\ \dot{\zeta}(t) + \alpha\zeta(t) &= \alpha\lambda\theta(x_t - k_x)\theta(\psi_t - 1),\end{aligned}\tag{6}$$

where $\eta = \gamma_x/\alpha k_y$ and $\lambda = \gamma_x\gamma_y/\alpha k_y$.

For the case of $x < k_x$, Eqs. (6) become a set of homogeneous ODEs with solutions that decay exponentially:

$$\begin{aligned}\psi(t)_{x < k_x} &= \psi_0 e^{-\alpha t}, \\ \zeta(t)_{x < k_x} &= \zeta_0 e^{-\alpha t}.\end{aligned}\tag{7}$$

Where, ψ_0 and ζ_0 are the initial conditions for the rescaled functions.

When $x > k_x$, we find

$$\psi(t)_{x > k_x} = \psi_0 e^{-\alpha t} + \eta (1 - e^{-\alpha t}).\tag{8}$$

Therefore, the solution for $\psi(t)$ converges to η as $t \rightarrow \infty$, similar to the solution of the discrete time equation presented in the main text.

On the other hand, the solution for $\zeta(t)$ also depends the values of ψ_0 and η . By carrying on a calculation similar to the one presented on the main text for the discrete time case, one finds:

$$\begin{aligned}\psi_0 > 1, \eta > 1 &\rightarrow \zeta(t)_{x > k_x} = \zeta_0 e^{-\alpha t} + \lambda(1 - e^{-\alpha t}), \\ \psi_0 > 1, \eta < 1 &\rightarrow \zeta(t)_{x > k_x} = \zeta_0 e^{-\alpha t} + \lambda(1 - e^{-\alpha t}) \quad \text{for } t \in \left\{0, 1, \dots, t_1 = \frac{1}{\alpha} \log \left(\frac{\psi_0 - \eta}{1 - \eta} \right)\right\}, \\ &\zeta(t)_{x > k_x} = \zeta_1 e^{-\alpha(t-t_1)} \quad \text{for } t > t_1, \\ \psi_0 < 1, \eta > 1 &\rightarrow \zeta(t)_{x > k_x} = \zeta_0 e^{-\alpha t} \quad \text{for } t \in \left\{0, 1, \dots, t_1 = \frac{1}{\alpha} \log \left(\frac{\eta - \psi_0}{\eta - 1} \right)\right\}, \\ &\zeta(t)_{x > k_x} = \zeta_1 e^{-\alpha(t-t_1)} + \lambda(1 - e^{-\alpha(t-t_1)}) \quad \text{for } t > t_1, \\ \psi_0 < 1, \eta < 1 &\rightarrow \zeta(t)_{x > k_x} = \zeta_0 e^{-\alpha t}.\end{aligned}\tag{9}$$

Here, $\zeta_1 = \zeta(t)|_{t=t_1}$.

Clearly, from the above solutions, the expression levels from genes Y and X do not synchronize, since $y(t) \neq z(t)$ as $t \rightarrow \infty$. In addition, $y(t)$ and $z(t)$ also do not reach oscillatory states, in accordance with the results of the discrete time model.

C. FFL with OR gate

We present the solution for the FFL [4, 20, 21] with an OR gate. We consider the coherent version cFFL where all regulations are activators. The discrete-time dynamics of expression levels y_t and z_t of genes Y and Z in the cFFL with a Boolean OR gate are given by the following pair of difference equations:

$$\begin{aligned} y_{t+1} &= (1 - \alpha)y_t + \gamma_x \theta(x_t - k_x), \\ z_{t+1} &= (1 - \alpha)z_t + \gamma_x \theta(x_t - k_x) + \gamma_y \theta(y_t - k_y), \end{aligned} \tag{10}$$

where α , γ_y , and γ_z have the same definition as in the main text. By adopting the same rescaled variables, $\psi_t = y_t/k_y$ and $\zeta_t = z_t/k_y$, we rewrite Eq. (10) as:

$$\begin{aligned} \psi_{t+1} &= \beta\psi_t + \alpha\eta\theta(x_t - k_x), \\ \zeta_{t+1} &= \beta\zeta_t + \alpha\lambda_x\theta(x_t - k_x) + \alpha\lambda_y\theta(\psi_t - 1), \end{aligned} \tag{11}$$

where we have $\beta = (1 - \alpha)$, $\eta = \gamma_x/\alpha k_y$, $\lambda_x = \gamma_x/\alpha k_y$, and $\lambda_y = \gamma_y/\alpha k_y$. Again, without lack of generality, we consider $x_t = x$ constant in time. Clearly, the solution for ψ_t is not affected by the OR gate, therefore, it depends only on the value of x and is given by:

$$\psi_t = \psi_0 e^{-t/\tau} + \eta(1 - e^{-t/\tau})\theta(x - k_x). \tag{12}$$

Again, $\tau = -\log(1 - \alpha)$. Thus, if $x < k_x$, ψ_t exponentially decays to zero. On the contrary, if $x > k_x$, ψ_t converges to η . The solution for ζ_t displays different solutions, depending on the combination of x and the initial value ψ_0 .

First, consider the case of $x < k_x$. For $\psi_0 < 1$, we find a solution that always decays as $\zeta_t = \zeta_0 e^{-t/\tau}$. When $\psi_0 > 1$, the solution for ζ_t is given by $\zeta_t = \zeta_0 e^{-t/\tau} + \lambda_y (1 - e^{-t/\tau})$. However, since $x < k_x$ and ψ_t exponentially decays, this solution is valid only until $t^* = \lceil \tau \log \psi_0 \rceil$, the instant that $\psi_{t^*} < 1$. As ψ_t decays, ζ_t also decays as $\zeta_t = \zeta_{t^*} e^{-(t-t^*)/\tau}$.

We consider next the case of $x > k_x$. In this case, ψ_t always converges to η . Therefore, the solution for ζ_t depends not only on ψ_0 , but also on η . For $\psi_0 < 1$ and $\eta < 1$, we find

that ζ_t converges to λ_x as $\zeta_t = \zeta_0 e^{-t/\tau} + \lambda_x (1 - e^{-t/\tau})$. However, if $\eta > 1$, this solution is not valid after $t^* = \lceil \tau \log(\psi_0 - \eta) / (1 - \eta) \rceil$, when $\psi_t > 1$. In this case, as ψ_t saturates to η , ζ_t converges to $\lambda_x + \lambda_y$ as $\zeta_t = \zeta_{t^*} e^{-(t-t^*)/\tau} + (\lambda_x + \lambda_y) (1 - e^{-(t-t^*)/\tau})$.

For the case of $\psi_0 > 1$ and $\eta > 1$, the rescaled variable ζ_t always converges to $\lambda_x + \lambda_y$ as $\zeta_t = \zeta_0 e^{-t/\tau} + (\lambda_x + \lambda_y) (1 - e^{-t/\tau})$. However, if $\eta < 1$, this solution ceases to be valid at $t^* = \lceil \tau \log((\eta - \psi_0) / (\eta - 1)) \rceil$. Therefore, for this case ζ_t converges to λ_x as $\zeta_t = \zeta_{t^*} e^{-(t-t^*)/\tau} + \lambda_x (1 - e^{-(t-t^*)/\tau})$.

From the discussion above, it is clear that the rescaled variables ψ_t and ζ_t neither synchronize nor oscillate. Extending this results to the original variables y_t and z_t , we conclude that the expression levels of the genes Y and Z also do not synchronize: $y_t \neq z_t$ when $t \rightarrow \infty$.

II. SATISFIED FEED-FORWARD FIBER: SAT-FFF

Below, we describe the solutions of the SAT FFF circuit in the discrete time continuous variable model and in the ODE model.

A. SAT-FFF discrete time model

The SAT-FFF is a Feed-Forward Fiber with activator autoregulation where all interactions are satisfied. That is, it does not present the phenomenon of frustration and the dynamics converges to a fixed point. This can be simply seen by considering gene X high, which makes also gene Y high and Z high too. Finally, the configuration satisfies the AR loop, so all bonds are satisfied. The SAT-FFF is constructed on top of the cFFL by the addition of an autoregulator loop on the Y gene, as depicted in Fig. 1E (main text) and S1 Fig. 1A. The discrete time dynamics of the SAT-FFF with a logic interaction term is given by:

$$\begin{aligned} y_{t+1} &= (1 - \alpha)y_t + \gamma_x \theta(x_t - k_x) \times \gamma_y \theta(y_t - k_y), \\ z_{t+1} &= (1 - \alpha)z_t + \gamma_x \theta(x_t - k_x) \times \gamma_y \theta(y_t - k_y). \end{aligned} \tag{13}$$

Note that the Heaviside function $\theta(y_t - k_y)$ represents the activator feedback on the autoregulation of the Y gene. We consider an AND gate for the interactions [4]. Analogous results can be obtained for OR gates or with an first-order ODE model. Writing down the set of equations for the rescaled variables $\psi_t = y_t/k_y$ and $\zeta_t = z_t/k_y$, we get:

$$\begin{aligned}\psi_{t+1} &= \beta\psi_t + \alpha\lambda\theta(x_t - k_x)\theta(\psi_t - 1), \\ \zeta_{t+1} &= \beta\zeta_t + \alpha\lambda\theta(x_t - k_x)\theta(\psi_t - 1).\end{aligned}\tag{14}$$

Here, we made use of $\lambda = \gamma_x\gamma_y/\alpha k_y$ and $\beta = (1 - \alpha)$. We note that, since the second term on the right-hand side of both equations are equal, the dynamical variables ψ_t and ζ_t must synchronize, as well as y_t and z_t . Again, considering $x_t = x$ constant, for $x < k_x$, the solutions for ψ_t and ζ_t are trivial: both variables decay exponentially as $\psi_t = \psi_0 e^{-t/\tau}$ and $\zeta_t = \zeta_0 e^{-t/\tau}$, where $\tau^{-1} = -\log(1 - \alpha)$. This behavior is shown by the red solid line in S1 Fig. S1B with $\psi_0 = 0.9$.

In terms of the iterative map, the dynamics of the SAT-FFF for the rescaled variable ψ_t with $x > k_x$ is:

$$\psi_{t+1} = \beta\psi_t + \alpha\lambda\theta(\psi_t - 1) \equiv f(\psi_t),\tag{15}$$

so we find

$$f^t(\psi) = f^{t-1}(\beta\psi)\theta(1 - \psi) + f^{t-1}(\beta\psi + \lambda)\theta(\psi - 1).\tag{16}$$

This iterative map $\psi_t = f(\psi_t)$ provides different solutions depending on ψ_0 . Similar to the case of $x < k_x$, if $\psi_0 < 1$, the solution decays to zero as $\psi_t = \psi_0 e^{-t/\tau}$. However, if $\psi_0 > 1$, there are two possibilities, depending on the values of $\lambda = \gamma_x\gamma_y/\alpha k_y$.

First, if $\lambda > 1$, the solution for both rescaled variables converges to λ as $\psi_t = \psi_0 e^{-t/\tau} + \lambda(1 - e^{-t/\tau})$ and $\zeta_t = \zeta_0 e^{-t/\tau} + \lambda(1 - e^{-t/\tau})$, such that $\psi_{t \rightarrow \infty} \rightarrow \lambda$ and $\zeta_{t \rightarrow \infty} \rightarrow \lambda$, as presented by the blue dash-dotted line in S1 Fig. S1B. For this case, we use $\psi_0 = 1.1$ and $\lambda = 2$.

For $\lambda < 1$, ψ_t approaches 1 at a time t^* given by

$$t^* = \left\lceil \frac{1}{\log(1 - \alpha)} \log \left(\frac{1 - \lambda}{\psi_0 - \lambda} \right) \right\rceil.\tag{17}$$

Then, for $t > t^*$, the solutions decay to zero as $\psi_t = e^{-(t-t^*)/\tau}$ and $\zeta_t = \zeta_{t^*} e^{1(t-t^*)/\tau}$. This behavior is presented on S1 Fig. S1B by the dashed green line, where we use $\psi_0 = 2$ and $\lambda = 0.9$. The rescaled variables ψ_t and ζ_t always synchronize, so do y_t and z_t . This can be proved by finding the difference $\epsilon_t = \psi_t - \zeta_t$. For all the cases discussed above, ϵ_t decays exponentially fast as $\epsilon_t = (\psi_0 - \zeta_0) e^{-t/\tau}$.

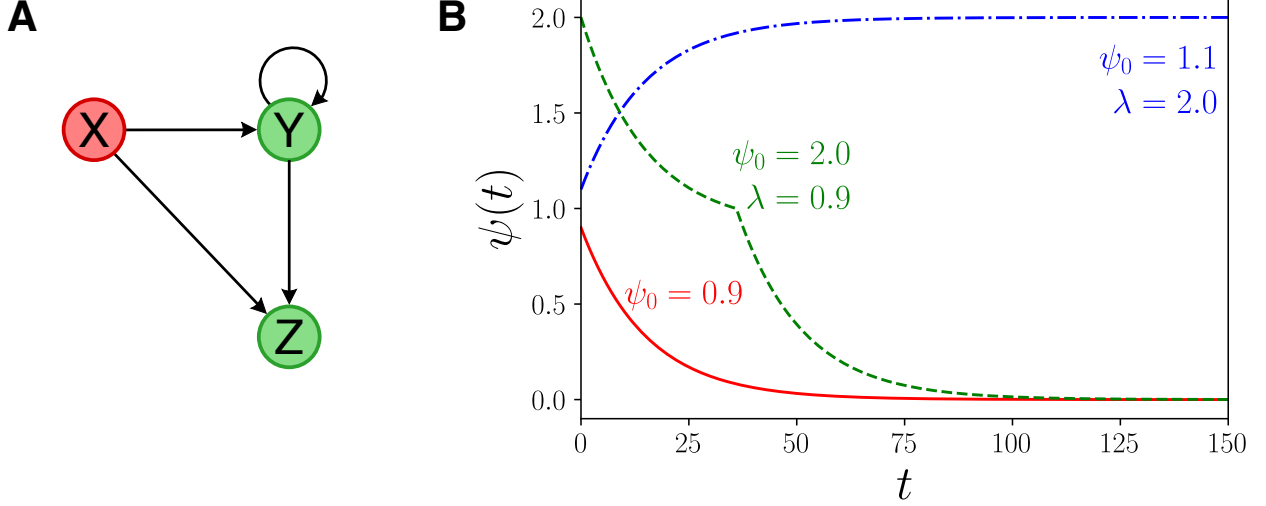


FIG. 1. **SAT-FFF.** **a**, Network representation of the SAT-FFF. All regulations are activators. **b**, Different behaviors for the analytical solutions of ψ_t depending on ψ_0 and λ , as discussed in the text.

Now, we can use the solution with x_t constant to qualitatively understand the SAT-FFF in general. An example of the SAT-FFF with non-constant x_t is depicted on Fig. 1F in the main text. As shown, variable y_t and z_t do synchronize but with no internal oscillations. We feed an external oscillatory pattern of x_t as a square wave. For $x_t < k_x$, both y_t and z_t decay exponentially. When $x_t > k_x$, they tend to saturate at $\gamma_x \gamma_y / \alpha$. The SAT-FFF synchronizes at a fixed point.

B. SAT-FFF ODE

Here, we consider the ODE model of SAT-FFF to confirm results presented in Section II A. The dynamics of gene X is driven by outside sources, so we only consider the dynamics of genes Y and Z which are described by equations:

$$\begin{cases} \dot{y} = -\alpha y(t) + \gamma_x \theta(x(t) - k_x) \times \gamma_y \theta(y(t) - k_y), \\ \dot{z} = -\alpha z(t) + \gamma_x \theta(x(t) - k_x) \times \gamma_y \theta(y(t) - k_y). \end{cases} \quad (18)$$

Taking $\psi(t) = y(t)/k_y$, $\zeta(t) = z(t)/k_y$ and $\delta = \gamma_x \gamma_y / k_y$ we transform Eq. (18) to:

$$\begin{cases} \dot{\psi} = -\alpha\psi(t) + \delta \theta(x(t) - k_x) \times \theta(\psi(t) - 1), \\ \dot{\zeta} = -\alpha\zeta(t) + \delta \theta(x(t) - k_x) \times \theta(\psi(t) - 1). \end{cases} \quad (19)$$

Without loss of generality, we consider the case of $x(t) = x$ constant in time. If $x < k_x$, then the solution of Eq. (19) is given by:

$$\begin{cases} \psi(t)_{x < k_x} = \psi_0 e^{-\alpha t}, \\ \zeta(t)_{x < k_x} = \zeta_0 e^{-\alpha t}, \end{cases} \quad (20)$$

where ψ_0 and ζ_0 are the initial conditions. Now, let's consider the case $x > k_x$. Equation (19) then transforms into:

$$\begin{cases} \dot{\psi} = -\alpha\psi(t) + \delta \theta(\psi(t) - 1) \\ \dot{\zeta} = -\alpha\zeta(t) + \delta \theta(\psi(t) - 1) \end{cases} \quad (21)$$

Due to the existence of isomorphic input trees between both genes, $\psi(t)$ and $\zeta(t)$ synchronize and therefore $y(t)$ and $z(t)$ synchronize also, so we only consider dynamics of the first equation:

$$\dot{\psi} = -\alpha\psi(t) + \delta \theta(\psi(t) - 1). \quad (22)$$

It's easy to see that for $\psi_0 < 1$, Eq. (20) will be the solution of Eq. (22). When $\psi_0 > 1$ and $\delta/\alpha > 1$, the solution is given by:

$$\psi(t) = \delta/\alpha + (\psi_0 - \delta/\alpha)e^{-\alpha t}. \quad (23)$$

In the case $\psi_0 > 1$ and $\delta/\alpha < 1$, the dynamics of ψ is split into two parts. One part before ψ decays to 1 and the other one after ψ crossed 1. The time when $\psi(t)$ crosses 1 is equal to:

$$t_c = \frac{1}{\alpha} \ln\left(\frac{\psi_0 - \delta/\alpha}{1 - \delta/\alpha}\right), \quad (24)$$

and the dynamics can be written as:

$$\begin{cases} t \in [0, t_c] & \psi(t) = \delta/\alpha + (\psi_0 - \delta/\alpha)e^{-\alpha t}, \\ t \in [t_c, \infty] & \psi(t) = \frac{\psi_0 - \delta/\alpha}{1 - \delta/\alpha} e^{-\alpha t}. \end{cases} \quad (25)$$

To summarize, the solution is:

$$\left\{ \begin{array}{ll} \psi_0 < 1 & \psi(t) = \psi_0 e^{-\alpha t} \\ \psi_0 > 1, \frac{\delta}{\alpha} > 1 & \psi(t) = \delta/\alpha + (\psi_0 - \delta/\alpha)e^{-\alpha t} \\ \psi_0 > 1, \frac{\delta}{\alpha} < 1 & \begin{cases} t \in [0, t_c] & \psi(t) = \delta/\alpha + (\psi_0 - \delta/\alpha)e^{-\alpha t} \\ t \in [t_c, \infty] & \psi(t) = \frac{\psi_0 - \delta/\alpha}{1 - \delta/\alpha} e^{-\alpha t}. \end{cases} \end{array} \right. \quad (26)$$

This solution is analogous to the one obtained for the discrete time model in Section II A.

III. UNSATISFIED FEED-FORWARD FIBER: UNSAT-FFF

Now, we turn our attention to the UNSAT-FFF. The solution of this circuit is developed in the main text using a discrete-time difference equation with a logistic interaction. Below we elaborate on the solution of the ODE continuum model and on the conditions on the period-amplitude relation and the clock functionality.

A. UNSAT-FFF ODE

The UNSAT-FFF circuit can be reduced to study the base of the circuit since both genes Y and Z synchronize their behaviour as shown in the main text. The base of this circuit is a negative autorregulation loop (Fig. 3) plus an external regulator given by X. This circuit has been synthetically implemented by Stricker *et al.* in Ref. [18] using a promoter that drives the expression in the absence of LacI (and acts as a negative feedback loop) or in the presence of IPTG, which acts as an activator. It was shown experimentally that this circuit leads to oscillatory behaviour in the expression profiles. This result was corroborated with a dynamical ODE model in [18] which here we adapt to study the case of the UNSAT-FFF with ODE. See also the review paper [53] for further reading.

Following the same approach as above, we consider gene $x(t) = x$ constant in time and larger than $x > k_x$, and rescale the expression of genes $y(t)$ and $z(t)$ as $\psi(t) = y(t)/k_y$ and

$\zeta(t) = z(t)/k_z$. Since genes $y(t)$ and $z(t)$ synchronize their activities, then only one equation needs to be considered, $\psi(t)$.

The key to observe oscillations in a first-order ODE is to consider the delay in the signal propagation in the circuit. Without delay the dynamics converge to a fixed point; no oscillatory solution exist in a first-order ODE continuum-time model. The situation is different in the discrete-time model considered in the text. In this case, a discrete time plus a logic approximation lead to oscillations.

Negative feedback loop circuits with delays have been widely investigated in the dynamical systems literature. Here, we adapt the negative feedback loop model with delay of Stricker *et al.* (see Eq. (6) in Supplementary Information in Ref. [18]). We consider delays in the negative feedback loop which is the key feature to explain the experimentally observed robust oscillation in this circuit [18].

Delays in a biological circuit arise from the combined processes of intermediate steps like transcription, translation, folding, multimerization and binding to DNA. This series of biological processes are lumped into a single arrow between two genes in the network representation of the circuit. In reality this arrow represents processes that should be modeled in detail. These biological processes can be approximately taken into account by a delay in the interaction term in the dynamical equations. The interaction term can be written as $\delta \theta(1 - \psi(t - \tau))$, where τ represents the delay caused by the fact that the process of self-repression is not instant. Therefore, the dynamics of $\psi(t)$ are described by a first-order delay-differential equation (DDE) [18] of the form:

$$\dot{\psi} = -\alpha\psi(t) + \delta \theta(1 - \psi(t - \tau)), \quad (27)$$

where τ represents the delay caused by expression process.

We derive analytical solutions to this equation following a procedure outlined in [54] (Chapter V). We start by noting that initial conditions used to solve a DDE are not given by the value of the function at one point, but rather by a set of values of the function on an interval of length τ . The solution of a DDE can't be thought of as a sequence of values of $\psi(t)$ as in an ODE, but rather as a set of functions $\{f_0(t), f_1(t), f_2(t), \dots, \}$, defined over a set of contiguous time intervals $\{[-\tau, 0], [0, \tau], [\tau, 2\tau], \dots, \}$.

Let's consider Eq. (27) with initial function $f_0(t)$ for $t \in [-\tau, 0]$. Then for $t \in [0, \tau]$ Eq. (27) looks like:

$$\dot{\psi} = -\alpha\psi(t) + \delta \theta(1 - f_0(t - \tau)). \quad (28)$$

Moving the degradation term to the left and multiplying by $e^{\alpha t}$ we get:

$$\dot{\psi}e^{\alpha t} + \alpha\psi(t)e^{\alpha t} = \delta e^{\alpha t}\theta(1 - f_0(t - \tau)). \quad (29)$$

Re-writing the left part, we obtain:

$$\frac{d(\psi e^{\alpha t})}{dt} = \delta e^{\alpha t}\theta(1 - f_0(t - \tau)), \quad (30)$$

and integrating on the interval \int_0^t , we get:

$$\psi e^{\alpha t} - \psi(0) = \delta \int_0^t e^{\alpha t'}\theta(1 - f_0(t' - \tau))dt'. \quad (31)$$

Considering that ψ is continuous at 0 ($\psi(0) = f_0(0)$) and $\psi(t)$ for $t \in [0, \tau]$ is given by $f_1(t)$:

$$f_1(t) = f_0(0)e^{-\alpha t} + \delta \int_0^t e^{\alpha(t'-t)}\theta(1 - f_0(t' - \tau))dt', \quad (32)$$

then, following the same procedure, we can derive the general formula for finding the solution $\psi(t)$ on the interval $[k\tau, (k+1)\tau]$, assuming that the solution on the previous interval $[(k-1)\tau, k\tau]$ is given by $f_{k-1}(t)$. We then need to solve the following iterative equation:

$$\dot{\psi} = -\alpha\psi(t) + \delta \theta(1 - f_{k-1}(t - \tau)). \quad (33)$$

The solution of this equation can be found by applying the integrating factor method integrating on $\int_{k\tau}^t$. We obtain:

$$\psi(t) = \psi(k\tau) * e^{\alpha(k\tau-t)} + \delta \int_{k\tau}^t e^{\alpha(t'-t)}\theta(1 - f_{k-1}(t' - \tau))dt'. \quad (34)$$

Using Eq. (34) we can recursively find functions $\{f_0(t), f_1(t), f_2(t), \dots, \}$ on the interval of interest, which provide the solution to Eq. (27). Using Wolfram Mathematica we find functions on the interval $t \in [-\tau, 30\tau]$ for $f_0 = 2$, $\alpha = 0.2$, $\delta = 1$ and $\tau = 1$ and put them together to find the solution plotted in S1 Fig. S2A.

We note from Eq. (34) that all functions f_k are written as the sum of an exponential function and a constant. By looking at Eq. (27), we see that when the Heaviside function

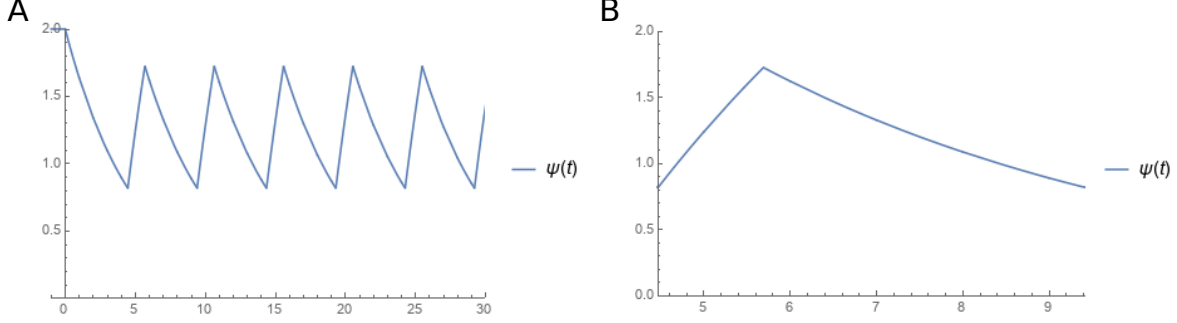


FIG. 2. **UNSAT-FFF delay ODE model.** **A**, Solution of Eq. (27) using recursive Eq. (34) on $t \in [-\tau, 30\tau]$ for $f_0 = 2$, $\alpha = 0.2$, $\delta = 1$ and $\tau = 1$. **B**, One period of the oscillation of solution in (A) consisting of two exponential pieces.

is equal to zero, we get a solution that decays exponentially to zero. Likewise, when the Heaviside function is equal to 1, we get a solution that exponentially grows to $\frac{\delta}{\alpha}$. In other words, the solution will grow until $\theta(1 - \psi(t - \tau))$ changes to zero (i.e., when $\psi(t - \tau) > 1$) and will decay until $\theta(1 - \psi(t - \tau))$ changes to one (i.e., when $\psi(t - \tau)$ will cross 1 again, but from different side). Therefore, we get oscillations consisting of two exponential pieces. One period of the oscillation is shown in S1 Fig. S2B. The solution on this interval is given by:

$$\begin{cases} t \in [4.47, 5.69] & \psi(t) = 5 - 10.2 * e^{-0.2t} \\ t \in [5.69, 9.42] & \psi(t) = 5.4 * e^{-0.2t}, \end{cases} \quad (35)$$

which is the predicted behavior. Additionally, we note that this circuit functions as a capacitor charging and discharging in an RC circuit.

B. Period-amplitude relationship

As shown in the main text, the solution of the discrete-time Boolean interaction model for $\lambda > 1$ oscillates in time, as well as the DDE considered in the previous section. Next, we show that this oscillation has a characteristic amplitude and period. First, to compute the amplitude of oscillations A_ψ for the rescaled variable ψ_t , we recall that the iterative map $\psi = f(\psi)$ satisfies the recursive equation:

$$f^t(\psi) = f^{t-1}(\beta\psi)\theta(\psi - 1) + f^{t-1}(\beta\psi + \alpha\lambda)\theta(1 - \psi). \quad (36)$$

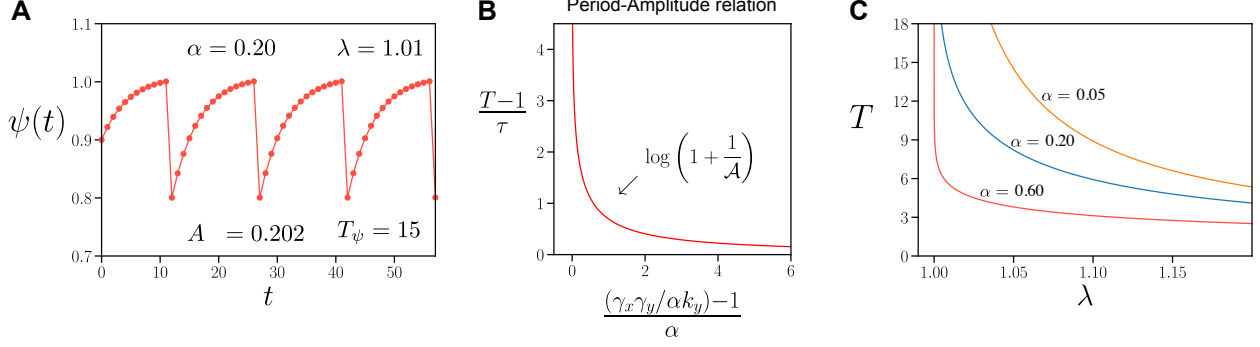


FIG. 3. Period-amplitude relationship. **a**, Solutions for $\alpha = 0.2$ and $\lambda = 1.01$. The values for $A_\psi = 0.202$ and $T = 15$ obtained with the use of Eq. (37) and Eq. (39) perfectly agree with the ones found by numerical simulations. **b**, Period-amplitude relationship in terms of the original set of parameters α , k_y , γ_x , and γ_y . **c**, Period of oscillations as a function of λ for different values of α .

Thus, the amplitude of oscillations A_ψ is given by

$$A_\psi = \lim_{\psi \rightarrow 1^-} f(\psi) - \lim_{\psi \rightarrow 1^+} f(\psi) = \alpha\lambda, \quad (37)$$

which implies that

$$A_\psi = \frac{\gamma_x \gamma_y}{k_y}. \quad (38)$$

To find the period T of the oscillations, we recall from Eq. (6) in the main text that the solution for the minimum value of ψ , $\psi_{\min} < 1$, evolves to its maximum value ψ_{\max} in $T - 1$ iterations as $\psi_{\max} = e^{-(T-1)/\tau} \psi_{\min} + \lambda(1 - e^{-(T-1)/\tau})$. Since $\psi_{\min} = (1 - \alpha)\psi_{\max}$, due to the fact that $\psi_{\max} > 1$, we find

$$T = \left[1 + \tau \log \left(1 + \frac{\alpha}{\lambda - 1} \right) \right], \quad (39)$$

where we used $\psi_{\max} = 1$. For example, using $\alpha = 0.2$ and $\lambda = 1.01$, we find $A_\psi = 2.02$ and $T = 15$, which agrees with the numerical simulation presented in S1 Fig. S3A.

Equation (39) allows to define a rescaled amplitude $\mathcal{A} = (\lambda - 1)/\alpha$, and a reduced period $\mathcal{T} = (T - 1)/\tau$ such that

$$\mathcal{T} = \log \left(1 + \frac{1}{\mathcal{A}} \right), \quad (40)$$

which corresponds to the *period-amplitude relationship* of the UNSAT-FFF. A plot of this relationship is shown in S1 Fig. S3B, where we plot $(T - 1)/\tau$ as a function of $[(\gamma_x \gamma_y / \alpha k_y) - 1] / \alpha$.

Coming back to the original variable $y_t = k_y \psi_t$, we have that the amplitude of oscillations of y_t , $A = k_y A_\psi$, is given by:

$$A = \gamma_x \gamma_y, \quad (41)$$

and from Eq. (39), we can write the period of oscillations as a function of the original set of parameters as

$$T = 1 - \frac{1}{\log(1 - \alpha)} \log \left(1 + \frac{\alpha}{(\gamma_x \gamma_y / \alpha k_y) - 1} \right). \quad (42)$$

S1 Figure S3C shows the period of oscillations T as a function λ for $\alpha = 0.60$, $\alpha = 0.20$, and $\alpha = 0.05$.

C. UNSAT-FFF clock functionality

The clock functionality of the UNSAT-FFF can be understood by analyzing its response function, i.e. the relation between oscillations at the input and at the output of the circuit. The amplitude A_y , and period T of the oscillations are not independent like in the harmonic oscillator, but are related through a ‘period-amplitude’ relation expressed by Eq. (40) and S1 Fig. S3B. From Eq. (42), for α sufficiently small,

$$T - 1 \sim \frac{k_y}{\gamma_x \gamma_y} = \frac{1}{A}, \quad (43)$$

which constrains the ‘clock’ (T) of the circuit to the power (A_y). As a consequence, A_y and T cannot be controlled arbitrarily, and this (A-T) constraint helps to stabilize the UNSAT-FFF response against disturbance in the input X. For example, for a given available power supply, the system is constrained to dissipate this power, and when the UNSAT-FFF oscillates, it is automatically set to operate on an extended time window (T large) at low amplitude A when a small expression level is required (A small) and vice-versa. Results for the clock functionality of the Fibonacci Fiber and $n = 2$ Fiber can be carried out in a similar manner. The idea is that Fibonacci fibers with longer and longer loops can carry more robust oscillatory patterns than simple autoregulation negative feedback loops.

IV. EXAMPLES OF SYMMETRY AND BROKEN SYMMETRY CIRCUITS

A. Symmetry circuits (*fibers*) from [24]

Our findings show that simple sub-graphs ubiquitous on gene regulatory networks are analogous to symmetric electronic circuits which can work as clocks, revealing a hierarchy of symmetry circuits. Here, we describe these symmetric circuits in more detail following [24]. Supplementary File 1 presents the full list of circuits found across the regulatory networks of *A. thaliana*, *M. tuberculosis*, *B. subtilis*, *E. coli*, *salmonella*, *yeast*, mouse and humans. Below we enumerate the set of symmetric *fibers* found in Ref. [24] in the genetic networks of these species.

1. Repressor regulator link (*stub*)

We start by an isolate repressor link. As depicted in Fig. 3A, this repressor regulator alone does not form an input tree, neither it forms a *base*. Since it works as a transistor, its logic representation is a NOT gate.

2. Repressor AR loop: $|1, 0\rangle$

In Fig. 3B, we show the repressor autoregulation loop. When a repressor link is found as an AR loop, we have a genetic network with one single loop ($n = 1$) and no external regulator ($\ell = 0$), which we denote symbolically by $|1, 0\rangle$. Such simple network has an input tree that feeds its own expression levels. Also, it is equivalent to its own *base*. By the analysis of the corresponding logical circuit, one can observe that it naturally oscillates, since it is a NOT gate that feeds itself.

3. UNSAT-FFF: $|1, 1\rangle$

The repressor autoregulation loop introduces a symmetry between Y and Z that allows the expression levels y_t and z_t to synchronize and oscillate. The increase of external regulators does not affect the complexity of UNSAT-FFF, since its dynamics remains restricted to the sole loop on the network. This can be verified in the corresponding input tree and in its

base. The collapse of Z into Y forms a *base* with $n = 1$ autoregulator and $\ell = 1$ external regulator. Because of the repressor feedback, the oscillation and synchronization of Y and Z are again evident in its logic circuit. In Fig. 3C, we use the NAND gate for representing gene Y and an AND gate for gene Z, but other gates (such as an OR logic gate) would result in similar conclusions.

4. *Fibonacci Fiber*: $|1.6180\dots, 0\rangle$

The Fibonacci Fiber shown in Fig. 3D is characterized by the addition of a second feedback loop. This regulatory network have a Fibonacci sequence $Q_t = Q_{t-1} + Q_{t-2}$ as an input tree. The branching structure of the input tree implies that the Fibonacci Fiber can store memory dynamically by the interaction with its past states, although it is continually erased in time. As shown in the logic circuit of Fibonacci Fiber, its structure can oscillate and synchronize, but is unable to store static information. This situation changes as soon as we allow symmetries to break, which leads to a number of genetic circuits, as those depicted in Fig. 4. In Fig. 3D, we show examples of the Fibonacci Fiber on regulatory networks of various species. Note the presence of its *base* in the network representation for *B. subtilis* (genes *tnrA* and *glnR*), *E. coli* (genes *uxuR* and *exuR*), *M. tuberculosis* (genes Rv0182c and Rv3286c), *Salmonella* (genes *marA* and *soxS*), *Yeast* (genes Tec1 and Ste12), and in two networks from human genetic network (the pair genes *PAX5* and *TP53*, for the first example, and gene *FOS* and *CREM*, for the second).

5. $n = 2$ *Fiber*: $|2, 0\rangle$

Starting from a Fibonacci Fiber, the addition of a second autoregulation on gene X results in a symmetric input tree. Besides, the genetic network of the $n = 2$ Fiber collapses into a *base* with a single gene with two autoregulations (Fig. 3E). From the corresponding logic circuit, one can conclude that it is possible to achieve synchronization between genes X, Y and Z. In Fig. 3E we show examples of the $n = 2$ Fiber from the regulatory networks of *B. subtilis* (the first with the pair of genes *lexA* and *rocR*, and the second with genes *hprT*, *tilS* and *ftsH*).

B. Symmetry breaking circuits

Figure 4 shows the procedure to generate broken symmetry circuits. As we discuss in the main text, this process starts by a replica symmetry operation where the *base* from a given symmetry circuit is duplicated. The symmetry is broken by the addition of two input genes as regulators of the circuit. The resulting broken symmetry circuits are analogous to flip-flops circuits from digital electronics. Such circuits are able to store memory statically, playing a central role in the design of microprocessors. In what follows, we describe the AR, FFF, and Fibonacci broken symmetry circuits and their analogous electronic circuits in detail. Supplementary File 1 presents the full list of circuits found across the regulatory networks of *A. thaliana*, *M. tuberculosis*, *B. subtilis*, *E. coli*, *salmonella*, *yeast*, mouse and humans.

1. AR symmetry breaking circuit: SR flip-flop

Through a replica symmetry duplication, gene Y ‘opens-up’ its AR loop into two mutually regulated genes Y and Y’. We break the symmetry relation between Y and Y’ by the inclusion of different inputs S and R as depicted in Fig. 4 (replica symmetry breaking), such that $S \neq R$.

The SR flip-flop does not provide synchronized outputs. After the input signals arrive at the logic gates, each gate provides its output without waiting for the output of the other. This results in fast oscillations which, in the particular application to integrated circuits in digital electronics, are undesired. Then, in digital electronics, the input $S = 0$ and $R = 0$ is said to be forbidden, since the NAND gates set both $Q = 1$ and $\bar{Q} = 1$, which violates the logical state $\bar{Q} = \text{not } Q$. In Fig. 4, we use the NAND gates, but the use of a NOR gates leads to similar conclusions.

Two biological realizations of the AR symmetry breaking class are shown in Fig. 4, both from human regulatory networks with genes *NFKB1* and *HOXA9* (upper), and the regulatory network of genes *IRF4* and *BCL6* (bottom). Gene *NFKB1* further regulates two genes, *BST1* and *HAX1* as its outputs, but this regulation does not affect the functionality of the flip-flop.

2. FFF symmetry breaking circuit: Clocked SR flip-flop

Following the same strategy, we start with the *base* of the UNSAT-FFF and symmetrize it through a replica symmetry duplication. Note that the replica symmetry of FFF adds a second level of NAND logic gates to the SR flip-flop via gene X. In order to have consistent logic operations, we add an input clock gene CLK which symbolizes the activation of gene X, since gene X needs to receive input for its activation. The resulting circuit is analogous to the Clocked SR flip-flop after the addition of the input genes S and R. The second level flip-flop inverts the outputs of the previous SR flip-flop logic circuit, meaning that when $S = 1$ and $R = 0$ ($S = 0$ and $R = 1$), the circuit outputs $Q = 1$ and $\bar{Q} = 0$ ($Q = 0$ and $\bar{Q} = 1$). The input $S = 0$ and $R = 0$ results in an unchanged state. When the input of gene CLK is low, $CLK = 0$, the output of the second level of both NAND gates outputs high signals, independently of the values of S and R, assuring that the outputs Q and \bar{Q} remain unchanged. However, when the clock input is $CLK = 1$, it allows the first level of NAND gates to change the outputs for $S \neq R$. The clocked SR flip-flop also has a forbidden state when $S = 1$ and $R = 1$ in digital electronics. In Fig. 4, we show two biological realizations of the FFF broken symmetry breaking circuit, the set of genes $\{CLOCK, NR0B2, NR3C1, E2F1$ and $TP53\}$ and the set $\{CEBPA, DDIT3, PRDM1, CEBPB$ and $MYC\}$, both examples are from human regulatory genetic networks. The outputs of the flip-flops, like $E2F1$ and $TP53$, further regulate a set of genes each as indicated by the red genes in the figure. These regulatory interactions do not affect the functionality of the flip-flops since they are outgoing links.

3. Fibonacci symmetry breaking circuit: JK flip-flop

The replica symmetry duplication of the Fibonacci Fiber results in a logic circuit similar to the FFF broken symmetry breaking circuit. However, the regulation links $Y \rightarrow X'$ and $Y' \rightarrow X$ yields a different logic circuit, which is analogous to the Clocked JK flip-flop, where the input genes are now J and K. The additional links solve the unpredictable output for the $J = 1$ and $K = 1$ case by commuting the values stored in Q and \bar{Q} . Two examples of the Fibonacci broken symmetry circuits are shown in Fig. 4 for the sets of genes $\{PITX1, JUN, NKX3-1, TP53$ and $ESR1\}$ and $\{FLI1, HDAC1, EPS300, AR$ and $RELA\}$, both from

human genetic networks. We also show the set of genes regulated by these flip-flops.

V. DESCRIPTION OF DATASETS

Datasets are described in S1 Table 1. We use a set of datasets of transcriptional regulatory networks found in the literature. All datasets are freely available from online sources. In Supplementary File 1 we present a plot of all found circuits. In the case of symmetric circuits, same colored nodes indicate the genes in the *fiber*. The external regulators are colored with different colors. We also present all the symmetry broken circuits across all species as indicated in the file. The statistics, count and Z-scores of the circuits are presented in Table 1 and 2 in the main text. The file with all circuits can be found at <https://bit.ly/2YM5x3H>.

VI. ALGORITHM TO FIND FIBERS

To obtain the set of nodes in the graph that belong to a *fiber*, we use the algorithm described in detail by Kamei and Cock [41] and developed in Ref. [24] to obtain the ‘*minimal balanced coloring*’ of the graph (referred as balanced coloring for simplicity), where we color the network by assigning a different color to each *fiber*.

To understand what balanced coloring means in the context of graph theory, we need to define the concept of input set (which is a part of the input tree). In a directed graph, the input set of a given node is the set of nodes with edges pointing into that node. Thus, the input set is the first layer of the input tree. Next, we define the Input Set Color Vector (ISCV) of a node as a vector of length equal to the number of colors in the graph, that is the number of *fibers*. Each entry of the ISCV of a given node counts how many nodes of each color are in the input set of this node. The balanced coloring is achieved by iteration by increasing the number of colors (length of ISCV) until all nodes of the same color have the same ISCVs. At this point, each color identifies each *fiber* in the graph.

Finding graph balanced coloring is equivalent to finding node sets with isomorphic input trees. A brief explanation of that is the following. If two nodes have the same ISCVs, nodes of their input sets have same colors. Thus these nodes are said to belong to the same equivalence class [41]. Inductively, the same can be said of the input set of the nodes in the input set. This recurrent relation implies that two nodes that have the same input sets will

Species	Database	Additional information
Arabidopsis Thaliana	ATRM [32]	We use high-confidence functionally confirmed transcriptional regulatory interactions from the ATRM database of the broadly used model plant Arabidopsis. http://atrm.cbi.pku.edu.cn/
Micobacterium Tuberculosis	Research article [33]	Supplementary Information of Ref. [33] https://www.ncbi.nlm.nih.gov/pmc/articles/PMC2600667/bin/msb200863-s2.xls
Bacillus subtilis	SubtiWiki [34]	We download the database from SubtiWiki website and consider all repressor and activation links as “Repression” and “Activation”. This database is considered the primary source of information for Bacillus. http://subtiwiki.uni-goettingen.de/
Escherichia coli	RegulonDB [35]	We use the TF - operon interaction network from [35]. RegulonDB combines transcriptional regulator interactions obtained by curating literature and using NLP high-quality data and partially confirmed experimentally and computationally predicted data. http://regulondb.ccg.unam.mx/
Salmonella SL1344	SalmoNet [36]	We use the regulatory layer of the strain Salmonella Typhimurium SL1344. SalmoNet consists of manually curated low-throughput and high-throughput experiments and predictions based on experimentally verified binding sites and TF-gene binding site data from RegulonDB. http://salmonet.org/
Yeast	YTRP [38]	We use the TF-gene regulatory and TF-gene binding networks. Results of the TFPEs (Transcription Factor Perturbation Experiments) identify the regulatory targets of TFs. This is further refined by using literature-curated data. http://cosbi3.ee.ncku.edu.tw/YTRP/Home
Mouse	TRRUST [39]	Downloaded from TRRUST website. TRRUST is constructed using sentence-based text mining of more than 20 million abstracts from research articles, refined by manual curation. https://www.grnpedia.org/trrust/
Human	TRRUST [39] TRRUST_2 [39] KEGG [40]	Downloaded from TRRUST website. Downloaded from TRRUST website and curated. We use KEGG API to download all pathways of Human gene regulatory network. After that, all networks are put together and duplicates are removed. https://www.genome.jp/kegg/pathway.html

TABLE 1. **Description of dataset acquisition.** All data are gathered from publicly available sources [32–40].

have isomorphic input trees and will belong to the same *fiber* (for rigorous proof see chapter 4 in [42]).

The algorithm to find balanced coloring was described in detail by Kamei and Cock [41]. In their algorithm, all nodes of the graph have the same initial color and, through a series of operations, they are recolored until balanced coloring is reached. The detailed description of the algorithm is as follows:

1. Initially, all nodes are assigned the same color.
2. Each node is assigned with the N -dimensional vector (ISCV), where N is current number of colors at the current iteration of the algorithm. Each entry of this vector is the number of nodes of certain color with ingoing link to the respective node. In the first iteration, $N = 1$ and each entry is the in-degree of the node.
3. If vectors for all nodes of the same color are equal, the balanced coloring is achieved and the algorithm stops.
4. Otherwise, if coloring is unbalanced, each unique vector is assigned a new color and the graph is recolored accordingly.
5. Steps 2-4 are repeated until condition in Step 3 is satisfied.

For example consider the FFF graph in S1 Fig. S4A. Initially, we assign the same color, white, to all nodes. Then, we assign a 1-dimensional vector to each node which counts the in-degree of each node (S1 Fig. S4B). Since ISCVs of X and Y (which have the same color) are different, $\text{ISCV}(X) = 0$ and $\text{ISCV}(Y) = 2$, where the entry refers to the number of inputs of white color, then the condition in Step 3 is not satisfied. There are two unique ISCVs, thus only two new colors are necessary. Thus, a 2-dimensional vector is assigned to each node: $\text{ISCV}(X) = (0, 0)$, $\text{ISCV}(Y) = (1, 1)$, and $\text{ISCV}(Z) = (1, 1)$. Here, the first entry refers to the number of inputs of green color and the second entry of red color. Thus, each entry of this vector is related to a new color, for example, red and green (see S1 Fig. S4D). Then, the network is recolored accordingly, as depicted in S1 Fig. S4C. At this step, $\text{ISCV}(Y)$ and $\text{ISCV}(Z)$ are the same, and different from the $\text{ISCV}(X)$, and both have the same color, also different from the color of X , therefore balanced coloring is reached and the algorithm stops. We provide an implementation of this algorithm at <https://github.com/makselab/fiberCodes>.

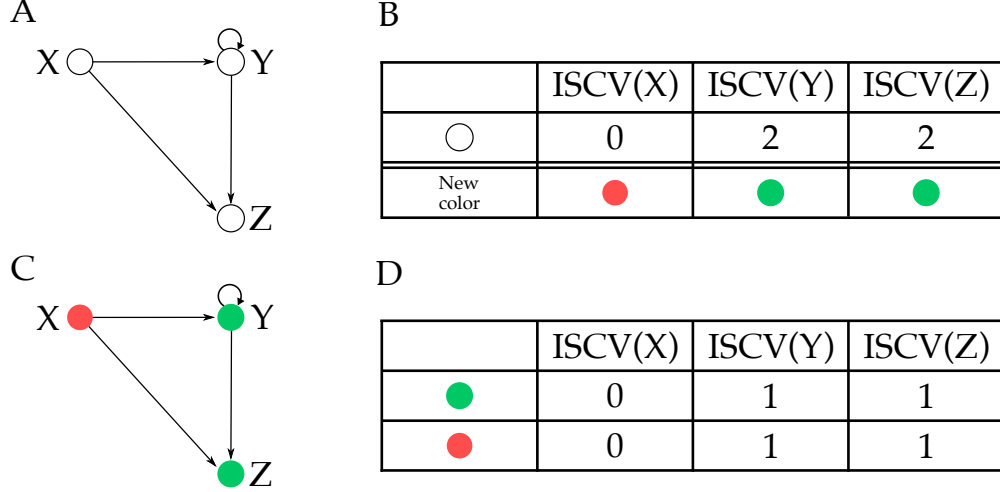


FIG. 4. Illustration of the balanced coloring algorithm to find *fibers*.

VII. ALGORITHM TO FIND BROKEN SYMMETRY CIRCUITS

To count the number of occurrences of broken symmetry circuits in a given graph we count the number of appearances of induced subgraphs as defined in Refs. [43–45]. Subgraphs and induced subgraphs are graph-theoretical concepts introduced in the social and computer sciences as applications to graph matching and pattern recognition [44]. We allow symmetry breaking to come from any gene in the circuit. Let's consider a graph $G = \{V, E\}$, where V is the set of nodes and E is the set of links. For instance in S1 Fig. S5A $V = \{A, B, C, D, Y, Y'\}$ and $E = \{A \rightarrow Y, Y \rightarrow B, Y \rightarrow Y', Y' \rightarrow Y, Y' \rightarrow C, D \rightarrow Y'\}$. A *subgraph* $G' = \{V', E'\}$ of a graph $G = \{V, E\}$ is a graph such that $V' \subset V$ and $E' \subset E$ [43]. For example S1 Fig. S5B is a subgraph of the graph in S1 Fig. S5A with $V' = \{Y, Y'\} \subset V$ and $E' = \{Y' \rightarrow Y\} \subset E$. An *induced subgraph* $G' = \{V', E'\}$ of a graph $G = \{V, E\}$ is a subgraph with a set of nodes $V' \subset V$ and all links $E' \subset E$ such that their heads and tails are in V' . For example the subgraph of S1 Fig. S5B is not induced graph of G since it is missing the link $\{Y \rightarrow Y'\}$. That is, S1 Fig. S5B is not an induced subgraph (but it is just a subgraph of G), because one of the links $\{Y \rightarrow Y'\}$ with endpoints in V' is missing. However the graph of S1 Fig. S5C is an induced subgraph of G since $V' = \{Y, Y'\}$ and $E' = \{Y \rightarrow Y', Y' \rightarrow Y\}$ are included, but links $\{A \rightarrow Y, Y \rightarrow B, Y' \rightarrow C, D \rightarrow Y'\}$ don't belong to G' . The problem of finding broken symmetry circuits consists on three steps: (1) identify a *base* and create a replica symmetry circuit, (2) find subgraphs isomorphic to the replica symmetry circuit, and (3) remove subgraphs that are not induced.

The first step is to find subgraphs isomorphic to the replica symmetry circuit. Let's consider an example. The matrix in S1 Fig. S5D represents the adjacency matrix A of the symmetric part of the SR flip-flop (i.e., a toggle switch). That is, A is the replica symmetry part (Fig. 4, third row) of the broken symmetry circuit. Similarly, S1 Fig. S5G,H show the adjacency matrices of clocked SR flip-flop and JK flip-flop circuits. The general idea is to choose a subgraph and check if it is isomorphic to the circuit and continue doing this for all possible subgraphs in the entire network. However, this task is computationally expensive. Even for circuits with 5 nodes, the computational time is N^5 , where N is the total number of nodes in G , which means that for big enough graphs the algorithm can take very long computational time. Different approaches to this problem have been widely studied and are nicely reviewed in Ref. [46]. Time costs can be cut if unprofitable paths are identified and skipped in the search space. One of the recent works in the field is the VF2 algorithm developed by Cordella *et al.* [47]. It is designed to deal with large graphs and uses state of the art techniques in order to reduce computational time. We use the algorithm implemented in a popular R package igraph [48] as a function `subgraph_isomorphisms(...)`. We provide the analysis and plotting scripts allowing to reproduce our results at <https://github.com/makselab/CircuitFinder>.

The second step is to remove all the subgraphs that are not induced or, simply speaking, have extra links between the genes in the broken symmetry circuit. We follow this procedure: take a node set identified above, find the induced subgraph of the complete graph with this node set and compare the adjacency matrix of the induced subgraph with the adjacency matrix of the circuit. If the matrices are different, then the circuit is removed. All remaining circuits are the broken symmetry flip-flops that we are looking for. Multi-links and self-loops are removed from the network prior to consideration.

By applying the steps described above we get the full list of induced subgraphs that are isomorphic to the given circuit.

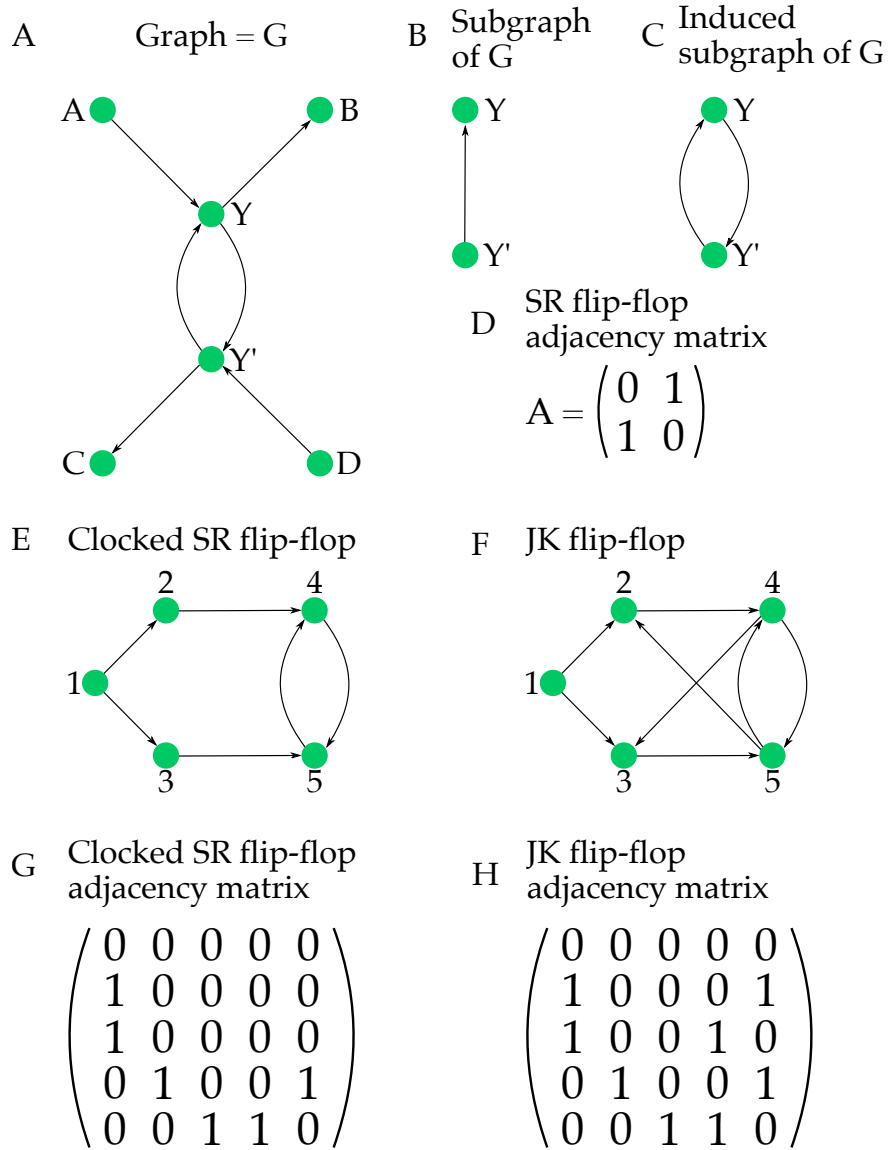


FIG. 5. Definition of the induced subgraph used to obtain the broken symmetry circuits. **A**, Graph G. **B**, Subgraph of G. **C**, Induced Subgraph of G. **D**, Adjacency matrix of SR flip-flop. **E**, Clocked SR flip-flop. **F**, JK flip-flop. **G**, Adjacency matrix of Clocked SR flip-flop. **H**, Adjacency matrix of JK flip-flop.

-
- [1] Hartwell LH, Hopfield JJ, Leibler S, Murray AW. From molecular to modular cell biology. *Nature*. 1999;402: C47-C52.
- [2] Milo R, Shen-Orr SS, Itzkovitz S, Kashtan N, Chklovskii D, Alon U. Network motifs: simple building blocks of complex networks. *Science*. 2002;298: 824-827.
- [3] Shen-Orr SS, Milo R, Mangan S, Alon U. Network motifs in the transcriptional regulation network of *Escherichia coli*. *Nature Genet*. 2002;31: 64-68.
- [4] Alon U. *An Introduction to Systems Biology: Design Principles of Biological Circuits*. Boca Raton: CRC Press; 2006.
- [5] Klipp E, Liebermeister W, Wierling C, Kowald A, Herwig R. *Systems Biology: a textbook*. Weinheim: Wiley-VCH; 2016.
- [6] Tyson JJ, Chen KC, Novak B. Sniffers, buzzers, toggles and blinkers: dynamics of regulatory and signaling pathways in the cell. *Curr Opin Cell Biol*. 2003;15(2): 221-31.
- [7] Monod J, Jacob F. General conclusions: teleonomic mechanisms in cellular metabolism, growth and differentiation. *Cold Spring Harb Symp Quant Biol*. 1961;26: 389-401.
- [8] Teo JY, Woo SS, Sarpeshkar R. *Synthetic Biology: A Unifying View and Review Using Analog Circuits*. *IEEE Trans. on Biomed. Circuits and Syst*. 2015;9: 453-474.
- [9] Dalchau N, Szé G, Hernansaiz-Ballesteros R, Barnes CP, Cardelli L, Phillips A, et al. Computing with biological switches and clocks. *Natural Computing*. 2018;17: 761-779.
- [10] Atkinson MR, Savageau MA, Myers JT, Ninfa AJ. Development of genetic circuitry exhibiting toggle switch or oscillatory behavior in *Escherichia coli*. *Cell*. 2003;113: 597-607.
- [11] Gardner TS, Cantor CR, Collins JJ. Construction of a genetic toggle switch in *Escherichia coli*. *Nature*. 2000;403: 339-342.
- [12] Kramer BP, Fussenegger M. Hysteresis in a synthetic mammalian gene network. *Proc Natl Acad Sci USA*. 2005;102: 9517-9522.
- [13] Kramer BP, Viretta AU, Baba MD-E, Aube D, Weber W, Fussenegger M. An engineered epigenetic transgene switch in mammalian cells. *Nature Biotech*. 2004;22: 867-870.
- [14] Guet CC, Elowitz MB, Hsing W, Leibler S. Combinatorial synthesis of genetic networks. *Science*. 2002;296: 1466-1470.
- [15] Ajo-Franklin CM, Drubin DA, Eskin JA, Gee EP, Landgraf D, Phillips I, et al. Rational design

- of memory in eukaryotic cells. *Genes Dev.* 2007;21: 2271-2276.
- [16] Ham TS, Lee SK, Keasling JD, Arkin AP. Design and construction of a double inversion recombination switch for heritable sequential genetic memory. *PLoS One.* 2008;3: e2815.
- [17] Elowitz MB, Leibler S. A synthetic oscillatory network of transcriptional regulators. *Nature.* 2000;403: 335-338.
- [18] Stricker J, Cookson S, Bennett MR, Mather WH, Tsimring LS, Hasty J. A fast, robust and tunable synthetic gene oscillator. *Nature.* 2008;456: 516-519.
- [19] Tigges M, Marquez-Lago TT, Stelling J, Fussenegger M. A tunable synthetic mammalian oscillator. *Nature.* 2009;457: 309-312.
- [20] Mangan S, Alon U. Structure and function of the feed-forward loop network motif. *Proc Natl Acad Sci USA.* 2003;100: 11980-11985.
- [21] Mangan S, Zaslaver A, Alon U. The coherent feedforward loop serves as a sign-sensitive delay element in transcription networks. *J Mol Biol.* 2003;334: 197-204.
- [22] Glass L, Kauffman SA. The logical analysis of continuous, non-linear biochemical control networks. *J Theor Biol.* 1973;38: 103-129.
- [23] Mangan S, Zaslaver A, Alon U. Negative autoregulation increases the input dynamic-range of the arabinose system of *Escherichia coli*. *BMC Sys Biol.* 2011;5: 111.
- [24] Morone F, Leifer I, Makse HA. Fibration symmetries uncover the building blocks of biological networks. Preprint at <https://bit.ly/2Z94B6o> (2019).
- [25] Golubitsky M, Stewart I. Nonlinear dynamics of networks: the groupoid formalism. *Bull Am Math Soc.* 2006;43: 305-364.
- [26] Boldi P, Vigna S. Fibrations of graphs. *Discrete Mathematics.* 2001;243: 21-66.
- [27] Anderson PW. The concept of frustration in spin glasses. *J of the Less-Common Metals.* 1978;62: 291-294.
- [28] Widlar RJ, Some circuit design techniques for linear integrated circuits. *IEEE Trans Circuit Theory.* 1965;4: 586-590. See also Widlar RJ: US Patent Number 3,320,439; Filed May 26, 1965; Granted May 16, 1967: Low-value current source for integrated circuits and Widlar RJ. Design techniques for monolithic operational amplifiers. *IEEE Solid-State Circuits.* 1969;4: 184-191.
- [29] Horowitz P, Hill W. *The Arts of Electronics.* 3rd ed. New York:Cambridge University Press; 2015.

- [30] Weinberg S. The Quantum Theory of Fields. Cambridge: Cambridge University Press; 2005.
- [31] Morone F, Makse HA. Symmetry group factorization reveals the structure-function relation in the *Caenorhabditis elegans* connectome. Nat Commun. 2019;10: 4961.
- [32] Jin J, He K, Tang X, Zhe L, Lv L, Zhao Y, et al. An Arabidopsis transcriptional regulatory map reveals distinct functional and evolutionary features of novel transcription factors. Mol Biol Evol. 2015;32: 1767-1773.
- [33] Balázsi G, Heath AP, Shi L, Gennaro ML. The temporal response of the Mycobacterium tuberculosis gene regulatory network during growth arrest. Mol Syst Biol. 2008;4: 225.
- [34] Zhu, B. & Stülke J. SubtiWiki in 2018: From genes and proteins to functional network annotation of the model organism *Bacillus subtilis*. Nucleic Acids Res. 2017;46: D743-D748.
- [35] Gama-Castro S, Salgado H, Santos A, Ledezma-Tejeida D, Muñiz-Rascado L, Santiago G-S, et al. RegulonDB version 9.0: High-level integration of gene regulation, coexpression, motif clustering and beyond. Nucleic Acids Res. 2015;44: D133-D143.
- [36] Métris A, Sudhakar P, Fazekas D, Demeter A, Ari E, Olbei M, et al. SalmoNet, an integrated network of ten *Salmonella enterica* strains reveals common and distinct pathways to host adaptation. NPJ Systems Biology and Applications. 2017;3: 31.
- [37] Cherry JM, Hong EL, Amundsen C, Balakrishnan R, Binkley G, Chan E, et al. Saccharomyces Genome Database: The genomics resource of budding yeast. Nucleic Acids Res. 2011;40: D700-D705.
- [38] Yang T-H, Wang C-C, Wang Y-C, Wu W-S. YTRP: a repository for yeast transcriptional regulatory pathways. Database 2014;2014: bau014.
- [39] Han H, Cho J-W, Lee S, Yun A, Kim H, Bae D, et al. TRRUST v2: An expanded reference database of human and mouse transcriptional regulatory interactions. Nucleic Acids Res. 2017;46: D380-D386.
- [40] Kanehisa M, Sato Y, Kawashima M, Furumichi M, Tanabe M. KEGG as a reference resource for gene and protein annotation. Nucleic Acids Res. 2015;44: D457-D462.
- [41] Kamei H, Cock PJ. A. Computation of balanced equivalence relations and their lattice for a coupled cell network. SIAM J Appl Dyn Syst. 2013;12: 352-382.
- [42] Aldis JW. A polynomial time algorithm to determine maximal balanced equivalence relations. Int J Bifurc Chaos Appl Sci Eng. 2008;18: 407-427.
- [43] Weisstein EW, "Subgraph". From MathWorld—A Wolfram Web Resource. <http://>

mathworld.wolfram.com/Subgraph.html

- [44] Harary F. Graph Theory. Reading: Addison-Wesley; 1994.
- [45] https://en.wikipedia.org/wiki/Induced_subgraph
- [46] Conte D, Foggia P, Sansone C, Vento M. Thirty years of graph matching in pattern recognition. *Int J Pattern Recognit Artif Intell.* 2004;18: 265-298.
- [47] Cordella LP, Foggia P, Sansone C, Vento M. A (sub)graph isomorphism algorithm for matching large graphs. *IEEE Trans Pattern Anal Mach Intell.* 2004;26: 1367-1372.
- [48] Csardi G, Nepusz T. The Igraph software package for complex network research. *Inter Journal, Complex Systems.* 2006;1695: 1-9.
- [49] Ingram PJ, Stumpf MP, Stark J. Network motifs: structure does not determine function. *BMC Genomic.* 2006;7: 108.
- [50] Payne JL, Wagner A. Function does not follow form in gene regulatory circuits. *Sci Rep.* 2015;5: 13015.
- [51] Macía J, Widder S, Solé R. Specialized or flexible feed-forward loop motifs: a question of topology. *BMC Syst Biol.* 2009;3: 84.
- [52] Ahnert SE, Fink TMA. Form and function in gene regulatory networks: the structure of network motifs determines fundamental properties of their dynamical state space. *J Royal Soc Interface.* 2016;13: 20160179.
- [53] Purcell O, Savery N, Grierson C, Di Bernardo M. A comparative analysis of synthetic genetic oscillators. *J Royal Soc Interface.* 2010;7: 1503-24.
- [54] Driver RD. Ordinary and delay differential equations. New York: Springer Verlag; 1977.